Available online at www.sciencedirect.com
SCIENCE DIRECT®
Journal of Computational Physics 208 (2005) 315–344
JOURNAL OF COMPUTATIONAL PHYSICS
www.elsevier.com/locate/jcp

A multi-state HLL approximate Riemann solver for ideal magnetohydrodynamics

Takahiro Miyoshi [a,*], Kanya Kusano [b]

[a] Department of Physical Science, Graduate School of Science, Hiroshima University, Higashi-Hiroshima 739-8526, Japan
[b] Earth Simulator Center, Japan Agency for Marine-Earth Science and Technology, Yokohama 236-0001, Japan

Received 15 November 2004; received in revised form 7 February 2005; accepted 18 February 2005
Available online 14 April 2005

Abstract

A new multi-state Harten–Lax–van Leer (HLL) approximate Riemann solver for the ideal magnetohydrodynamic (MHD) equations is developed based on the assumption that the normal velocity is constant over the Riemann fan. This assumption is same as that used in the HLLC ("C" denotes Contact) approximate Riemann solver for the Euler equations. From the assumption, it is naturally derived that the Riemann fan should consist of four intermediate states for $B_x \neq 0$, whereas the number of the intermediate states is reduced to two when $B_x = 0$. Since the intermediate states satisfied with all jump conditions in this approximate Riemann system are analytically obtained, the multi-state HLL Riemann solver can be constructed straightforwardly. It is shown that this solver can exactly resolve isolated discontinuities formed in the MHD system, and hence named as HLLD Riemann solver. (Here, "D" stands for Discontinuities.) It is also analytically proved that the HLLD Riemann solver is positively conservative like the HLLC Riemann solver. Indeed, the HLLD Riemann solver corresponds to the HLLC Riemann solver when the magnetic field vanishes. Numerical tests demonstrate that the HLLD Riemann solver is more robust and efficient than the linearized Riemann solver, and its resolution is equally good. It indicates that the HLLD solver must be useful in practical applications for the ideal MHD equations.

Keywords: Magnetohydrodynamics; Approximate Riemann solver; HLL; HLLC; HLLD; Positivity

1. Introduction

The magnetohydrodynamic (MHD) equations are the basic equations to represent macroscopic phenomena in various fields such as laboratory, space, and astrophysical plasmas, and the development of

* Corresponding author.
E-mail address: miyoshi@sci.hiroshima-u.ac.jp (T. Miyoshi).

0021-9991/$ - see front matter © 2005 Elsevier Inc. All rights reserved.
doi:10.1016/j.jcp.2005.02.017

accurate, efficient, and robust numerical schemes for MHD becomes increasingly important. Particularly, in space and astrophysical plasmas, it can often happen that the density becomes rather low and the internal energy is less dominant than the kinetic energy and, in some cases, the magnetic energy. The physical solutions of the MHD equations possess a positivity preserving property such that positive densities and positive pressures must be retained in every situation. However, numerical simulations for such low density plasmas sometimes generate unphysical solutions of negative densities or negative pressures. Therefore, robustness of the MHD scheme is quite important for practical applications with realistic parameters.

In order to obtain accurate numerical solutions for the ideal MHD equations, Brio and Wu [4] first developed the Roe-type linearized Riemann solver [26] for MHD with $\gamma = 2$. For general γ, construction of the Roe-type matrix and corresponding Roe-type average, which are more elaborate than those for $\gamma = 2$, has been pursued, for instance, by Cargo and Gallice [5] or Balsara [1]. Practically, an arithmetic average was often utilized instead of the Roe average, and it seems to work well [27]. Although the linearized Riemann solver for MHD is considerably more complicated than for the Euler equations and less efficient than "classical" MHD schemes such as Lax–Wendroff, it is accurate and robust enough and also efficient in comparison with the nonlinear Riemann solver [6,27]. Thus, the linearized Riemann solver might be a standard solver for the practical MHD simulations at present (e.g., [18,22,25,28]).

However, it has been shown that any linearization of certain Riemann problems for the Euler equations will yield a negative density or pressure, and therefore, no linearized Riemann solver for the Euler equations can maintain the positivity of density and pressure in every situation [9]. Moreover, the linearized Riemann solvers for MHD become more problematic than for the Euler equations in terms of positivity because negative pressures may be produced by numerical errors of not only the kinetic energy but also the magnetic energy.

As for the Euler solvers, the positivity preserving property is assured by variants of the flux vector splitting (FVS) method [12], the Harten–Lax–van Leer (HLL) approximate Riemann solver [9] and the HLLC Riemann solver (where "C" stands for Contact wave) [2]. These schemes are said to be positively conservative. Particularly, we notice that the HLLC Riemann solver where the intermediate states in the Riemann fan are separated into two intermediate states by a contact discontinuity can resolve isolated contact discontinuities exactly. The other positively conservative schemes cannot resolve those discontinuities and, as a consequence, are quite dissipative.

On the other hand, for MHD, appropriate FVS schemes equivalent to the Euler equations have not been constructed so far partly because the flux function of the MHD equations is not homogeneous of degree one in the vector of the conservative variables. The positivity preserving property of the HLL Riemann solver for MHD was investigated by Janhunen [16], where the MHD equations are modified to allow numerical magnetic monopoles, and confirmed from the extensive numerical experiments. Recently, Gurski [13] extended the HLLC Riemann solver of the Euler equations to the MHD equations and proposed an HLLC-type MHD Riemann solver and a modified version of the HLLC solver called smooth HLLC. The smooth HLLC was thought to be more accurate than the HLLC-type solver and a positively conservative variant of Linde's two-state approximate Riemann solver [20,21]. Independently, Li [19] also presented another variant of the HLLC-type Riemann solver for MHD. However, those solvers may not exactly resolve isolated rotational discontinuities probably due to the two-state approximation in the Riemann fan, although the HLLC-type Riemann solvers are more efficient than the standard linearized Riemann solver. As a result, it seems that the numerical resolution of the HLLC-type MHD solvers is not comparable with that of the linearized solver except for fast and entropy waves.

Thus, the previous schemes that are positively conservative for MHD are not satisfactory with respect to resolution, although the positivity preserving property is quite important in practical applications. Therefore, in this paper, a new scheme for the MHD equations is developed, which can satisfy the requirements of both positivity and high resolution nearly comparable to the linearized Riemann solver. The new solver is constructed by extending the HLL and the HLLC solvers for the Euler equations. Although there is

another essential problem for multi-dimensional MHD concerned with the violation of the divergence constraint (see, e.g., [8,16]), discussions of positivity here are restricted to one-dimensional MHD. Our HLL based solver for MHD can exactly resolve not only isolated contact discontinuities but also all other isolated discontinuities formed in the ideal MHD system, and therefore, the solver is named as HLLD.

The organization of the paper is as follows: After introduction, the MHD equations and their nature are presented in Section 2. We briefly review the single-state and two-state HLL approximate Riemann solvers in Sections 3 and 4. In Section 5.1, new multi-state approximate Riemann solver for MHD, called HLLD solver, is proposed. The important properties of the HLLD solver such as an exact resolution of discontinuities and a positivity preserving property are argued in Sections 5.2 and 5.3. In Section 6, several numerical tests are performed, and those results are discussed. Finally, concluding remarks are given in Section 7.

2. Governing equations

General one-dimensional hyperbolic conservation laws can be written as

$$\frac{\partial \mathbf{U}}{\partial t}+\frac{\partial \mathbf{F}}{\partial x}=0, \tag{1}$$

where all eigenvalues of the Jacobian $A=\partial\mathbf{F}/\partial\mathbf{U}$ are real and distinct, and the set of corresponding eigenvectors is complete. In one-dimensional ideal MHD equations, the conservative variable vector $\mathbf{U}$ and the flux function $\mathbf{F}$ are given by

$$\mathbf{U}=\begin{pmatrix}\rho\\ \rho u\\ \rho v\\ \rho w\\ B_y\\ B_z\\ e\end{pmatrix},\quad \mathbf{F}=\begin{pmatrix}\rho u\\ \rho u^2+p_{\mathrm{T}}-B_x^2\\ \rho vu-B_xB_y\\ \rho wu-B_xB_z\\ B_yu-B_xv\\ B_zu-B_xw\\ (e+p_{\mathrm{T}})u-B_x(\mathbf{v}\cdot\mathbf{B})\end{pmatrix}, \tag{2}$$

where $\mathbf{v}=(u, v, w)$, $\mathbf{B}=(B_x, B_y, B_z)$, p_{T} denotes the total pressure, and other notations are standard. Here, due to the divergence free condition of the magnetic field, B_x is given as a constant in one dimension. The pressure p and the total pressure p_{T} are given by

$$p=(\gamma-1)\left(e-\frac{1}{2}\rho|\mathbf{v}|^2-\frac{1}{2}|\mathbf{B}|^2\right)\quad\text{and}\quad p_{\mathrm{T}}=p+\frac{1}{2}|\mathbf{B}|^2,$$

respectively.

It is well known that these equations have seven eigenvalues which correspond to two Alfvén waves, four magneto-acoustic (two fast and two slow) waves, and one entropy wave:

$$\lambda_{2,6}=u\mp c_{\mathrm{a}},\quad \lambda_{1,7}=u\mp c_{\mathrm{f}},\quad \lambda_{3,5}=u\mp c_{\mathrm{s}},\quad \lambda_4=u, \tag{3}$$

where

$$c_{\mathrm{a}}=\frac{|B_x|}{\sqrt{\rho}},\quad c_{\mathrm{f,s}}=\left\{\frac{\gamma p+|\mathbf{B}|^2\pm\sqrt{\left(\gamma p+|\mathbf{B}|^2\right)^2-4\gamma pB_x^2}}{2\rho}\right\}^{1/2}.$$

It is obvious that the inequalities

$$\lambda_1 \leqslant \lambda_2 \leqslant \lambda_3 \leqslant \lambda_4 \leqslant \lambda_5 \leqslant \lambda_6 \leqslant \lambda_7$$

are satisfied, and thus, some eigenvalues may coincide depending on the direction and the strength of the magnetic field. Therefore, the MHD equations are not strictly hyperbolic, and, as a consequence, the complete set of the eigenvectors is not obtained straightforwardly [1,4,5]. In addition, as first pointed out by Brio and Wu [1], the flux function $\mathbf{F}$ is not convex in the vector $\mathbf{U}$ in the MHD system.

Since the MHD equations possess non-convexity as well as non-strict hyperbolicity, a solution of the Riemann problem may be composed not only of ordinary shock and rarefaction waves but also other waves as compound waves and overcompressible shocks [4,17]. Although it is not so easy to solve the Riemann problem for such MHD system in general, the discontinuous solutions formed by the regular waves can be discussed easily using the Rankine–Hugoniot relations, $S[\mathbf{U}] = [\mathbf{F}]$, where S denotes the speed of the discontinuities and $[\cdot]$ indicates the jump of the states ahead of and behind the discontinuities, $\mathbf{U}_1$ and $\mathbf{U}_2$. When we consider solutions for which $u_1, u_2 \neq S$, i.e., there is net particle transport across the discontinuities, and $B_x \neq 0$, three types of shock solutions are obtained. In the cases of the compressible solutions, that is, $\rho_1 < \rho_2$ and $u_1 > u_2$, the fast and slow shocks are realized, in which both shocks conserve the signs of the tangential components of the magnetic field. While the magnetic field is strengthened behind the fast shock, it is weakened behind the slow shock. On the other hand, the incompressible condition for which $\rho_1 = \rho_2$ and $u_1 = u_2$ gives the following relations:

$$[\rho] = [p] = \left[B_y^2 + B_z^2\right] = 0, \quad \pm\sqrt{\rho}[v] = [B_y], \quad \pm\sqrt{\rho}[w] = [B_z], \tag{4}$$

across the discontinuity which moves with the Alfvén wave speed λ_2 or λ_6. This solution is called the Alfvén shock. Since thermodynamical quantities, ρ and p, are not changed across the discontinuity, it is also called the *rotational discontinuity*. Also, the discontinuity moving with the entropy wave speed λ_4 must be satisfied with

$$[B_y] = [B_z] = [v] = [w] = [p] = 0 \tag{5}$$

for the case of $B_x \neq 0$, or

$$\left[p + \frac{B_y^2 + B_z^2}{2}\right] = 0 \tag{6}$$

for $B_x = 0$. The former discontinuity is called the *contact discontinuity*. At the contact discontinuity, the tangential components of the velocity and magnetic field must be continuous. The latter relation, on the other hand, indicates that the tangential velocity and the tangential magnetic field may have a jump across the discontinuity. Thus, that is called the *tangential discontinuity*.

3. HLL Riemann solver

Let us consider general hyperbolic conservation laws (1), where $\mathbf{U}$ and $\mathbf{F}$ are not specified here. The integral form of the conservation laws for a rectangle $(x_1, x_2) \times (t_1, t_2)$ is given by

$$\int_{x_1}^{x_2} \mathbf{U}(x, t_2)\mathrm{d}x - \int_{x_1}^{x_2} \mathbf{U}(x, t_1)\mathrm{d}x + \int_{t_1}^{t_2} \mathbf{F}(\mathbf{U}(x_2, t))\mathrm{d}t - \int_{t_1}^{t_2} \mathbf{F}(\mathbf{U}(x_1, t))\mathrm{d}t = 0. \tag{7}$$

Harten et al. [15] showed that the Godunov-type scheme for (1) can be written in conservative form:

$$\mathbf{U}_i^{n+1} = \mathbf{U}_i^n - \frac{\Delta t}{\Delta x}\left[\mathbf{F}\left(\mathbf{R}(0;\mathbf{U}_i^n,\mathbf{U}_{i+1}^n)\right) - \mathbf{F}\left(\mathbf{R}(0;\mathbf{U}_{i-1}^n,\mathbf{U}_i^n)\right)\right],$$

where n and i indicate a time step and a cell number, respectively, and $\mathbf{R}(x/t;\mathbf{U}_i^n,\mathbf{U}_{i+1}^n)$ is the approximate solution of the Riemann problem around the interface $x_{i+1/2}$. In this form, the appropriate numerical fluxes are obtained by applying the integral conservation laws (7) over the rectangle $(x_i, x_{i+1/2})\times(t^n, t^{n+1})$ as

$$\mathbf{F}_{i+1/2} = \mathbf{F}_i - \frac{1}{\Delta t}\int_{x_i}^{x_{i+1/2}} \mathbf{R}\left(\frac{x - x_{i+1/2}}{\Delta t};\mathbf{U}_i^n,\mathbf{U}_{i+1}^n\right)\mathrm{d}x + \frac{x_{i+1/2} - x_i}{\Delta t}\mathbf{U}_i^n, \tag{8}$$

where $\mathbf{F}_{i+1/2} = \mathbf{F}(\mathbf{R}(0;\mathbf{U}_i^n,\mathbf{U}_{i+1}^n)), \mathbf{F}_i = \mathbf{F}(\mathbf{U}_i^n)$, and $\Delta t = t^{n+1} - t^n$. We note that the exact solution of the Riemann problem $\mathbf{R}_{\text{exact}}$ produces the fluxes of the original Godunov scheme. The numerical fluxes $\mathbf{F}_{i+1/2}$ obtained by the other integral conservation laws over $(x_{i+1/2}, x_{i+1})\times(t^n, t^{n+1})$ must coincide with (8) due to the consistency with the integral form of conservation laws over $(x_i, x_{i+1})\times(t^n, t^{n+1})$.

Particularly, Harten et al. [15] proposed one of the simplest Godunov-type scheme, the so-called HLL approximate Riemann solver. The HLL Riemann solver is constructed by assuming an average intermediate state between the fastest and slowest waves. Consider a "subsonic" solution of the single-state approximate Riemann problem at the interface between the left and right states, $\mathbf{U}_\mathrm{L}$ and $\mathbf{U}_\mathrm{R}$, where the minimum signal speed S_L and the maximum signal speed S_R are negative and positive, respectively (Fig. 1). By applying the integral conservation laws (7) over the Riemann fan, $(\Delta t S_\mathrm{L}, \Delta t S_\mathrm{R})\times(0, \Delta t)$, the intermediate state is given by

$$\mathbf{U}^* = \frac{S_\mathrm{R}\mathbf{U}_\mathrm{R} - S_\mathrm{L}\mathbf{U}_\mathrm{L} - \mathbf{F}_\mathrm{R} + \mathbf{F}_\mathrm{L}}{S_\mathrm{R} - S_\mathrm{L}}. \tag{9}$$

After that, as denoted by (8), the integral over $(\Delta t S_\mathrm{L}, 0)\times(0, \Delta t)$ gives the HLL fluxes,

$$\mathbf{F}^* = \frac{S_\mathrm{R}\mathbf{F}_\mathrm{L} - S_\mathrm{L}\mathbf{F}_\mathrm{R} + S_\mathrm{R}S_\mathrm{L}(\mathbf{U}_\mathrm{R} - \mathbf{U}_\mathrm{L})}{S_\mathrm{R} - S_\mathrm{L}}. \tag{10}$$

If both signal speeds are of the same sign, the fluxes must be evaluated only from the upstream side. Therefore, in general, the HLL fluxes become

$$\mathbf{F}_\mathrm{HLL} = \begin{cases} \mathbf{F}_\mathrm{L} & \text{if } S_\mathrm{L} > 0, \\ \mathbf{F}^* & \text{if } S_\mathrm{L} \leqslant 0 \leqslant S_\mathrm{R}, \\ \mathbf{F}_\mathrm{R} & \text{if } S_\mathrm{R} < 0. \end{cases} \tag{11}$$

Practically, (11) can be unified with (10) if the signal speeds are replaced by $S_\mathrm{L} = \min(S_\mathrm{L}, 0)$ and $S_\mathrm{R} = \max(S_\mathrm{R}, 0)$.

In order to complete the HLL Riemann solver, S_R and S_L must be estimated appropriately. Correctly speaking, the upper and lower bounds of the signal speed in the system cannot be obtained without information of the exact Riemann solution [2]. Particularly, the difficulty for the MHD equations may be

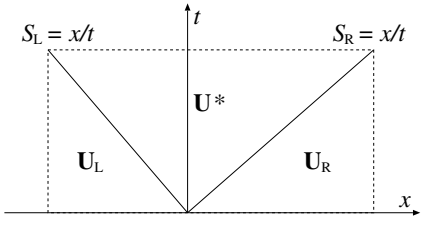

Fig. 1. Schematic structure of the Riemann fan with one intermediate state.

increased because bounded waves are capable of compound waves. Therefore, we should determine the algorithm as exactly as possible so as not to underestimate the minimum and maximum signal speeds. For example, Davis [7] gave those speeds as

$$\begin{aligned} S_{\mathrm{L}} &= \min\left[\lambda_1(\mathbf{U}_{\mathrm{L}}), \lambda_1(\mathbf{U}_{\mathrm{R}})\right], \\ S_{\mathrm{R}} &= \max\left[\lambda_m(\mathbf{U}_{\mathrm{L}}), \lambda_m(\mathbf{U}_{\mathrm{R}})\right], \end{aligned} \tag{12}$$

or Einfeldt et al. [9] used the algorithm as

$$\begin{aligned} S_{\mathrm{L}} &= \min\left[\lambda_1(\mathbf{U}_{\mathrm{L}}), \lambda_1\left(\mathbf{U}^{\mathrm{Roe}}\right)\right], \\ S_{\mathrm{R}} &= \max\left[\lambda_m\left(\mathbf{U}^{\mathrm{Roe}}\right), \lambda_m(\mathbf{U}_{\mathrm{R}})\right], \end{aligned} \tag{13}$$

where λ_1 and λ_m are the smallest and largest eigenvalues of (1), and $\lambda_j(\mathbf{U}^{\mathrm{Roe}})$ denotes the eigenvalue of the Roe matrix. Although these are not correct bounds of the signal speed [2], these algorithms seem to be highly effective. Indeed, the HLL solver for the Euler equations with appropriate choices for S_{L} and S_{R} is extremely robust since it satisfies an entropy inequality automatically [7] and ensures a positivity preserving property [9]. The robustness of the HLL solver is also expected for the MHD equations [16].

However, the HLL solver cannot resolve isolated discontinuities and, as a result, is quite dissipative because the solution of the Riemann problem is approximated by one intermediate state. Therefore, it is a natural thought that the single-state approximation should be extended to a two-state approximation in order to be more accurate while maintaining the nice properties.

4. Two-state HLL Riemann solver

4.1. HLLC Riemann solver for the Euler equations

In this subsection, we devote attention to the solver for the Euler equations, which are obtained by setting the magnetic field to zero in (2). In [15], it was suggested that a two-state approximate Riemann solver could be constructed to exactly resolve isolated contact discontinuities as well as isolated shocks although that was not implemented practically. However, Toro et al. [29] proposed a simple implementation of the two-state HLL Riemann solver for the Euler equations.

Consider the approximate Riemann problem in the Riemann fan which is separated into the left and the right intermediate states, $\mathbf{U}^*_{\mathrm{L}}$ and $\mathbf{U}^*_{\mathrm{R}}$, by the contact wave, S_M, as shown in Fig. 2. Toro et al. [29] assumed that the normal component of the velocity is constant over the Riemann fan, that is,

$$u^*_{\mathrm{L}} = u^*_{\mathrm{R}} = S_M.$$

Particularly, Batten et al. [2] insisted that S_M should be evaluated from the HLL average (9) as

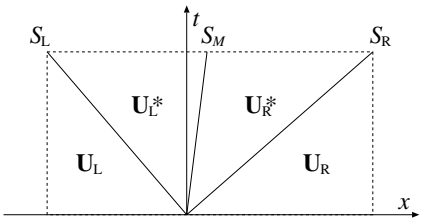

Fig. 2. Schematic structure of the Riemann fan with two intermediate states.

$$S_M = \frac{(\rho u)^*}{\rho^*} = \frac{(S_R - u_R)\rho_R u_R - (S_L - u_L)\rho_L u_L - p_R + p_L}{(S_R - u_R)\rho_R - (S_L - u_L)\rho_L}, \tag{14}$$

where S_L and S_R are estimated by (12) or (13). Once S_M is given by (14), the jump conditions across the S_α wave,

$$S_\alpha \mathbf{U}_\alpha^* - \mathbf{F}_\alpha^* = S_\alpha \mathbf{U}_\alpha - \mathbf{F}_\alpha, \tag{15}$$

where α = L or R, give the pressure in the Riemann fan as

$$\begin{aligned} p^* &= p_L^* = p_L + \rho_L(S_L - u_L)(S_M - u_L) \\ &= p_R^* = p_R + \rho_R(S_R - u_R)(S_M - u_R). \end{aligned} \tag{16}$$

These equalities are consistent with the fact that the pressure does not change across the contact discontinuity. Also, other intermediate states are derived from (15):

$$\rho_\alpha^* = \rho_\alpha \frac{S_\alpha - u_\alpha}{S_\alpha - S_M}, \tag{17}$$

$$v_\alpha^* = v_\alpha, \tag{18}$$

$$w_\alpha^* = w_\alpha, \tag{19}$$

$$e_\alpha^* = \frac{(S_\alpha - u_\alpha)e_\alpha - p_\alpha u_\alpha + p^* S_M}{S_\alpha - S_M}. \tag{20}$$

Thus, we obtain the complete set of $\mathbf{U}_\alpha^*$ and $\mathbf{F}_\alpha^*$. It is certain that the jump condition across the middle wave S_M is satisfied. Since the integral conservation laws over $(S_L\Delta t, 0)\times(0, \Delta t)$ for $S_M \geqslant 0$ and $(0, S_R\Delta t)\times(0, \Delta t)$ for $S_M \leqslant 0$ coincide with (15), the two-state HLL fluxes become

$$\mathbf{F}_{\mathrm{HLLC}} = \begin{cases} \mathbf{F}_L & \text{if } S_L > 0, \\ \mathbf{F}_L^* & \text{if } S_L \leqslant 0 \leqslant S_M, \\ \mathbf{F}_R^* & \text{if } S_M \leqslant 0 \leqslant S_R, \\ \mathbf{F}_R & \text{if } S_R < 0. \end{cases} \tag{21}$$

This solver is called HLLC Riemann solver since the HLLC solver can resolve isolated contact discontinuities exactly [2,29].

Batten et al. [2] showed that the HLLC solver is positively conservative if the conditions,

$$S_L < u_L - \sqrt{\frac{\gamma - 1}{2\gamma}} a_L, \quad S_R > u_R + \sqrt{\frac{\gamma - 1}{2\gamma}} a_R \tag{22}$$

where a is the sound speed $\sqrt{\gamma p/\rho}$, are satisfied. These are the same conditions as those for the single-state HLL Riemann solver shown by Einfeldt et al. [9] exactly and always satisfied by the estimates of (12) or (13).

4.2. HLLC-type Riemann solver for the MHD equations

Before constructing the new solver, some approaches to the extension of the HLLC Riemann solver for the Euler equations to the MHD equations are worth reviewing and discussing.

Recently, Gurski [13] developed the HLLC-type Riemann solver for ideal MHD, where the Riemann fan is separated into two intermediate states, $\mathbf{U}_L^*$ and $\mathbf{U}_R^*$, in the same way as the HLLC Riemann solver. As an

estimation of S_L and S_R, the algorithm (13) is adopted. Also, the middle wave S_M is evaluated from the HLL average like the HLLC. In MHD, the total pressure must be continuous across the middle wave instead of the pressure in the Euler equations as found from (5) or (6). Therefore, (16) is replaced by

$$\begin{aligned} p_T^* &= p_{T_L} + \rho_L(S_L - u_L)(S_M - u_L) \\ &= p_{T_R} + \rho_R(S_R - u_R)(S_M - u_R). \end{aligned} \tag{23}$$

Since the normal velocity in the Riemann fan is assumed to be constant, the densities in the intermediate states ρ_α^* are given by the same as the HLLC Riemann solver, (17). In the case of $B_x = 0$, the tangential momentum equations of MHD coincide with those of the Euler equations. Also, the tangential components of the magnetic field behave like passive scalars. Therefore, in this case, the intermediate states,

$$v_\alpha^* = v_\alpha, \tag{24}$$

$$w_\alpha^* = w_\alpha, \tag{25}$$

$$B_{y_\alpha}^* = B_{y_\alpha}\frac{S_\alpha - u_\alpha}{S_\alpha - S_M}, \tag{26}$$

$$B_{z_\alpha}^* = B_{z_\alpha}\frac{S_\alpha - u_\alpha}{S_\alpha - S_M}, \tag{27}$$

$$e_\alpha^* = \frac{(S_\alpha - u_\alpha)e_\alpha - p_{T_\alpha}u_\alpha + p_T^* S_M}{S_\alpha - S_M}, \tag{28}$$

are easily obtained by the similar procedure for the HLLC solver. In the case of $B_x \neq 0$, on the other hand, the intermediate states from (24)–(28) are not consistent with the jump condition on the contact discontinuity (5) in which the tangential components of the velocity and magnetic field must be continuous. Therefore, those are replaced by the HLL average (9) as

$$v_L^* = v_R^* = \frac{(\rho v)^*}{\rho^*} \equiv v^*, \tag{29}$$

$$w_L^* = w_R^* = \frac{(\rho w)^*}{\rho^*} \equiv w^*, \tag{30}$$

$$B_{y_L}^* = B_{y_R}^* = B_y^*, \tag{31}$$

$$B_{z_L}^* = B_{z_R}^* = B_z^*, \tag{32}$$

$$e_\alpha^* = \frac{(S_\alpha - u_\alpha)e_\alpha - p_{T_\alpha}u_\alpha + p_T^* S_M + B_x(\mathbf{v}_\alpha \cdot \mathbf{B}_\alpha - \mathbf{v}^* \cdot \mathbf{B}^*)}{S_\alpha - S_M}. \tag{33}$$

Finally, $\mathbf{F}_\alpha^*$ are computed from each jump condition. This solver is referred to as HLLC-G Riemann solver in this paper.

It is found that the fluxes obtained by (29)–(33) are not reduced to those by (24)–(28) in the limit of $B_x = 0$, and partly correspond to the single-state HLL fluxes. Therefore, the HLLC-G Riemann solver cannot simulate the structures related to the Alfvén and slow waves with high enough resolution although isolated contact discontinuities as well as isolated fast shocks can be resolved exactly.

In order to resolve the discontinuities across the slow and Alfvén waves sharply, Gurski [13] also proposed another method, as it were *extended* HLLC-type solver, where the intermediate states are obtained

by the jump conditions on S_α (15) properly. (These intermediate states will be shown later explicitly by (44)–(48) in subsection 5.1.) Although these are reduced to (24)–(28) in the case of $B_x = 0$, the jump condition across the middle wave is not satisfied, and thus, the conservation laws in the Riemann fan are broken in the sense of HLL-type solver. Consequently, as shown in Fig. 5 of [13], unphysical oscillations are produced even in the simple one-dimensional shock tube test. To remove these oscillations, a certain dissipation was also introduced in analogy with Linde's Riemann solver [20,21].

As another approach to recover the resolution of the HLLC-G solver and to suppress unphysical oscillations in the *extended* HLLC-type solver, by introducing the following form of the intermediate tangential velocities as

$$v_\alpha^* = v_\alpha + \frac{B_x\left(B_{y_\alpha} - B_y^*\right)}{\rho_\alpha(S_\alpha - u_\alpha)}, \tag{34}$$

$$w_\alpha^* = w_\alpha + \frac{B_x\left(B_{z_\alpha} - B_z^*\right)}{\rho_\alpha(S_\alpha - u_\alpha)}, \tag{35}$$

instead of (29) and (30), Li [19] constructed another HLLC-type Riemann solver for MHD, referred to as HLLC-L Riemann solver in this paper. The intermediate states of the HLLC-L solver are consistent with the integral of the conservation laws over the Riemann fan as opposed to the *extended* HLLC-type solver. Also, the HLLC-L solver naturally returns to the HLLC solver in the limit of zero magnetic field. We note, however, that the HLLC-L solver does not necessarily satisfy the jump condition on the contact discontinuity (5) due to the definitions (34) and (35). This fact does not mean that the HLLC-L solver cannot resolve isolated contact discontinuities exactly. In addition, since (31) and (32) are still used as the intermediate states of the magnetic field even in the HLLC-L solver, (26) and (27) cannot be realized in the limit where B_x becomes zero.

4.3. Linde's Riemann solver for hyperbolic conservation laws

Another two-state HLL Riemann solver was constructed by Linde [20,21]. In this solver, the jump of the intermediate states are connected with the jump of the left and the right states empirically by

$$\mathbf{U}_\mathrm{R}^* - \mathbf{U}_\mathrm{L}^* = \beta(\mathbf{U}_\mathrm{L}, \mathbf{U}_\mathrm{R})(\mathbf{U}_\mathrm{R} - \mathbf{U}_\mathrm{L}), \quad 0 \leqslant \beta \leqslant 1, \tag{36}$$

where β becomes 1 if an isolated discontinuity is detected in the Riemann fan, whereas β is 0 if the intermediate states are continuous. Thus, β is considered as a strength of the middle wave. Then, Linde's fluxes are derived by substituting (36) into the integral conservation laws over the two-state approximate Riemann fan as

$$\mathbf{F}_\alpha^* = \frac{S_\mathrm{R}\mathbf{F}_\mathrm{L} - S_\mathrm{L}\mathbf{F}_\mathrm{R} + (1-\beta)S_\mathrm{R}S_\mathrm{L}(\mathbf{U}_\mathrm{R} - \mathbf{U}_\mathrm{L}) + \beta S_\alpha S_M(\mathbf{U}_\mathrm{R} - \mathbf{U}_\mathrm{L})}{S_\mathrm{R} - S_\mathrm{L}}. \tag{37}$$

We find at once that Linde's fluxes return to the single-state HLL fluxes (10) when β becomes zero.

Since S_M and β are not specified in particular, it is obvious that the ability of the Linde solver is strongly dependent on the choice of S_M and β. In [20], S_M and β are given by the Roe average of the normal velocity and a heuristic linear function with respect to a gap from the jump condition, $S_M\Delta\mathbf{U} - \Delta\mathbf{F}$, while those are obtained through the least-squares solution of the jump condition with appropriate rescaling in [21]. Particularly, the latter method does not need any information about the eigensystem for the conservation laws. Thus, one can construct various versions of the Linde solver by introducing some adequate S_M and β.

Gurski [13] indicated that the expressions of the HLLC Riemann fluxes can be reformulated similar to Linde's fluxes. This is not surprising because the Linde solver may include any two-state Riemann solver

due to the arbitrariness of S_M and β. The reformulation of the HLLC-type MHD solver inspired that the *extended* HLLC-type solver which is accurate but oscillatory can be modified so as to smooth unwanted oscillations while preserving the positivity of density and pressure [13]. In this solver, named as smooth HLLC MHD solver, S_M is given by the HLL average and β is computed from $A^{*-1}\Delta\mathbf{W}^* = \beta A^{-1}\Delta\mathbf{W}$ instead of (36), where $\Delta\mathbf{W}$ possesses the unit of momentum and a certain linearization as $\Delta\mathbf{U} = A^{-1}\Delta\mathbf{W}$ is assumed. The smooth HLLC MHD solver is thought to be a positively conservative variant of the Linde solver.

The advantage of Linde's method is that the algorithm of the solver is independent of the details of the governing equations despite the exact resolution of isolated contact discontinuities. However, necessary and sufficient conditions of β to eliminate numerical oscillations completely have not been presented yet, and some class of Linde's fluxes may generate unphysical oscillations. Therefore, the Linde solver should be applied for a complex system without detail knowledge of its characteristics rather than the well-known system as the Euler equations and the MHD equations [21].

5. Multi-state HLL Riemann solver

5.1. HLLD Riemann solver for the MHD equations

The HLLC-type Riemann solvers for MHD as reviewed in the previous section may have some inconsistency with respect to the jump conditions without a particular treatment. We suppose that the HLLC-type solvers may include inconsistency between the assumption of constant normal velocity and the two-state approximation of the intermediate states in the Riemann fan. Therefore, in this subsection, the multi-state (more than two-state) HLL Riemann solver for the MHD equations is constructed based on the same basic assumption as that in the HLLC Riemann solver for the Euler equations.

Assume that the normal velocity is constant over the Riemann fan. Our assumption which is the same as in the HLLC solver [2,29] leads to the following noticeable conclusions: The normal velocity in the Riemann fan corresponds to the speed of the middle (entropy) wave. The total pressure is constant over the Riemann fan. Slow shocks cannot be formed inside the Riemann fan. Rotational discontinuities propagating with the Alfvén waves, on the other hand, may be generated. The latter two conclusions suggest that, in order to construct a more accurate HLL Riemann solver for MHD than the single-state HLL solver, the Riemann fan may be divided into four intermediate states, $\mathbf{U}_{\mathrm{L}}^{*}, \mathbf{U}_{\mathrm{L}}^{**}, \mathbf{U}_{\mathrm{R}}^{**}$, and $\mathbf{U}_{\mathrm{R}}^{*}$, as illustrated in Fig. 3. Therefore, we consider the approximate Riemann problem in the four-state Riemann fan separated by one entropy and two Alfvén waves, S_M and $S_{\mathrm{L}}^{*}, S_{\mathrm{R}}^{*}$.

The choice of S_M, in the present solver, is to evaluate the average normal velocity from the HLL average (9) as Batten et al. [2], Gurski [13] and Li [19] did:

$$S_M = \frac{(S_{\mathrm{R}} - u_{\mathrm{R}})\rho_{\mathrm{R}} u_{\mathrm{R}} - (S_{\mathrm{L}} - u_{\mathrm{L}})\rho_{\mathrm{L}} u_{\mathrm{L}} - p_{\mathrm{T_R}} + p_{\mathrm{T_L}}}{(S_{\mathrm{R}} - u_{\mathrm{R}})\rho_{\mathrm{R}} - (S_{\mathrm{L}} - u_{\mathrm{L}})\rho_{\mathrm{L}}}, \tag{38}$$

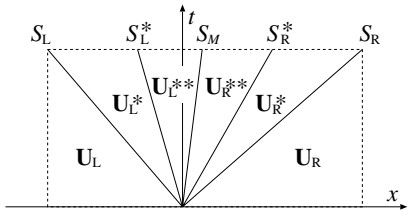

Fig. 3. Schematic structure of the Riemann fan with four intermediate states.

which is identical to (14) except that p is replaced by p_{T}. Since the normal velocity is assumed to be constant over the Riemann fan, the equalities

$$u_{\mathrm{L}}^{*} = u_{\mathrm{L}}^{**} = u_{\mathrm{R}}^{**} = u_{\mathrm{R}}^{*} = S_M \tag{39}$$

are given. In addition to (39), our assumption will restrict the total pressure to constant as

$$p_{\mathrm{T_L}}^{*} = p_{\mathrm{T_L}}^{**} = p_{\mathrm{T_R}}^{**} = p_{\mathrm{T_R}}^{*} = p_{\mathrm{T}}^{*}. \tag{40}$$

The average total pressure p_{T}^{*} in the Riemann fan should be evaluated consistent with the jump conditions for each wave. The present choice of S_M (38) consistently gives the equalities that $p_{\mathrm{T}}^{*} = p_{\mathrm{T_L}}^{*} = p_{\mathrm{T_R}}^{*}$ from the jump conditions of the normal momentum across S_{R} and S_{L} as indicated by (23) for the HLLC-type solver. More explicitly, (23) can also be rewritten as

$$p_{\mathrm{T}}^{*} = \frac{(S_{\mathrm{R}} - u_{\mathrm{R}})\rho_{\mathrm{R}} p_{\mathrm{T_L}} - (S_{\mathrm{L}} - u_{\mathrm{L}})\rho_{\mathrm{L}} p_{\mathrm{T_R}} + \rho_{\mathrm{L}}\rho_{\mathrm{R}}(S_{\mathrm{R}} - u_{\mathrm{R}})(S_{\mathrm{L}} - u_{\mathrm{L}})(u_{\mathrm{R}} - u_{\mathrm{L}})}{(S_{\mathrm{R}} - u_{\mathrm{R}})\rho_{\mathrm{R}} - (S_{\mathrm{L}} - u_{\mathrm{L}})\rho_{\mathrm{L}}}. \tag{41}$$

The other equalities $p_{\mathrm{T_L}}^{**} = p_{\mathrm{T_R}}^{**} = p_{\mathrm{T}}^{*}$ are also satisfied automatically as shown later. Note that contact, tangential, and rotational discontinuities can be formed in the Riemann fan even under the restriction (40).

Once S_M and p_{T}^{*} are given, the states $\mathbf{U}_{\alpha}^{*}$ neighboring $\mathbf{U}_{\alpha}$ are obtained from the jump conditions across S_{α},

$$S_{\alpha}\begin{pmatrix} \rho_{\alpha}^{*} \\ \rho_{\alpha}^{*} S_M \\ \rho_{\alpha}^{*} v_{\alpha}^{*} \\ \rho_{\alpha}^{*} w_{\alpha}^{*} \\ B_{y_{\alpha}}^{*} \\ B_{z_{\alpha}}^{*} \\ e_{\alpha}^{*} \end{pmatrix} - \begin{pmatrix} \rho_{\alpha}^{*} S_M \\ \rho_{\alpha}^{*} S_M^2 + p_{\mathrm{T}}^{*} - B_x^2 \\ \rho_{\alpha}^{*} v_{\alpha}^{*} S_M - B_x B_{y_{\alpha}}^{*} \\ \rho_{\alpha}^{*} w_{\alpha}^{*} S_M - B_x B_{z_{\alpha}}^{*} \\ B_{y_{\alpha}}^{*} S_M - B_x v_{\alpha}^{*} \\ B_{z_{\alpha}}^{*} S_M - B_x w_{\alpha}^{*} \\ (e_{\alpha}^{*} + p_{\mathrm{T}}^{*}) S_M - B_x (\mathbf{v}_{\alpha}^{*} \cdot \mathbf{B}_{\alpha}^{*}) \end{pmatrix} = S_{\alpha}\begin{pmatrix} \rho_{\alpha} \\ \rho_{\alpha} u_{\alpha} \\ \rho_{\alpha} v_{\alpha} \\ \rho_{\alpha} w_{\alpha} \\ B_{y_{\alpha}} \\ B_{z_{\alpha}} \\ e_{\alpha} \end{pmatrix} - \begin{pmatrix} \rho_{\alpha} u_{\alpha} \\ \rho_{\alpha} u_{\alpha}^2 + p_{\mathrm{T}_{\alpha}} - B_x^2 \\ \rho_{\alpha} v_{\alpha} u_{\alpha} - B_x B_{y_{\alpha}} \\ \rho_{\alpha} w_{\alpha} u_{\alpha} - B_x B_{z_{\alpha}} \\ B_{y_{\alpha}} u_{\alpha} - B_x v_{\alpha} \\ B_{z_{\alpha}} u_{\alpha} - B_x w_{\alpha} \\ (e_{\alpha} + p_{\mathrm{T}_{\alpha}}) u_{\alpha} - B_x (\mathbf{v}_{\alpha} \cdot \mathbf{B}_{\alpha}) \end{pmatrix}, \tag{42}$$

where α = L or R as used in the previous section. It is certain that the second equation of (42) is consistent with our choice of S_M and p_{T}^{*} because p_{T}^{*} itself is derived from this equation. The first equation of (42) gives

$$\rho_{\alpha}^{*} = \rho_{\alpha}\frac{S_{\alpha} - u_{\alpha}}{S_{\alpha} - S_M}, \tag{43}$$

which is identical to (17) except for the expression of S_M. Solving the third and fifth equations of (42) simultaneously, one obtains that

$$v_{\alpha}^{*} = v_{\alpha} - B_x B_{y_{\alpha}}\frac{S_M - u_{\alpha}}{\rho_{\alpha}(S_{\alpha} - u_{\alpha})(S_{\alpha} - S_M) - B_x^2}, \tag{44}$$

$$B_{y_{\alpha}}^{*} = B_{y_{\alpha}}\frac{\rho_{\alpha}(S_{\alpha} - u_{\alpha})^2 - B_x^2}{\rho_{\alpha}(S_{\alpha} - u_{\alpha})(S_{\alpha} - S_M) - B_x^2}. \tag{45}$$

Also, from the fourth and sixth equations, we obtain that

$$w_{\alpha}^{*} = w_{\alpha} - B_x B_{z_{\alpha}}\frac{S_M - u_{\alpha}}{\rho_{\alpha}(S_{\alpha} - u_{\alpha})(S_{\alpha} - S_M) - B_x^2}, \tag{46}$$

$$B_{z_{\alpha}}^{*} = B_{z_{\alpha}}\frac{\rho_{\alpha}(S_{\alpha} - u_{\alpha})^2 - B_x^2}{\rho_{\alpha}(S_{\alpha} - u_{\alpha})(S_{\alpha} - S_M) - B_x^2}. \tag{47}$$

Note that the numerical operations of 0/0 seem to appear in (44)–(47) if $S_M = u_\alpha$, $S_\alpha = u_\alpha \pm c_{f\alpha}$, $B_{y_\alpha} = B_{z_\alpha} = 0$, and $B_x^2 \geqslant \gamma p_\alpha$. In these cases, (44)–(47) can be simply replaced by $v_\alpha^* = v_\alpha, w_\alpha^* = w_\alpha$, and $B_{y_\alpha}^* = B_{z_\alpha}^* = 0$ since there is no shock across S_α i.e., $\rho_\alpha^* = \rho_\alpha$, $u_\alpha^* = u_\alpha$, and $p_{T_\alpha}^* = p_{T_\alpha}$. Finally, the seventh equation of (42) with (44)–(47) gives e_α^* as

$$e_\alpha^* = \frac{(S_\alpha - u_\alpha)e_\alpha - p_{T_\alpha}u_\alpha + p_T^* S_M + B_x(\mathbf{v}_\alpha \cdot \mathbf{B}_\alpha - \mathbf{v}_\alpha^* \cdot \mathbf{B}_\alpha^*)}{S_\alpha - S_M}. \tag{48}$$

The expressions (44)–(48) are the same than those employed for the intermediate states of the *extended* HLLC-type Riemann solver for MHD [13].

Subsequently, the inner intermediate states $\mathbf{U}_\alpha^{**}$ are considered. From the jump condition of the continuity equation across an arbitrary S where $S_L < S < S_M$ or $S_M < S < S_R$,

$$\rho_\alpha^{**} = \rho_\alpha^*, \tag{49}$$

because of the relation (39). When (49) is given, the jump condition for the normal momentum across S leads to

$$p_{T_\alpha}^{**} = p_{T_\alpha}^*. \tag{50}$$

Thus, (40) is satisfied. Also from (49), it is appropriate that the propagation speeds of the Alfvén waves (3) in the intermediate states are evaluated by

$$S_L^* = S_M - \frac{|B_x|}{\sqrt{\rho_L^*}}, \quad S_R^* = S_M + \frac{|B_x|}{\sqrt{\rho_R^*}}. \tag{51}$$

Although we should consider the other jump conditions across S_α^* waves, the jump conditions,

$$S_\alpha^* \begin{pmatrix} \rho_\alpha^* v_\alpha^{**} \\ \rho_\alpha^* w_\alpha^{**} \\ B_{y_\alpha}^{**} \\ B_{z_\alpha}^{**} \end{pmatrix} - \begin{pmatrix} \rho_\alpha^* v_\alpha^{**} S_M - B_x B_{y_\alpha}^{**} \\ \rho_\alpha^* w_\alpha^{**} S_M - B_x B_{z_\alpha}^{**} \\ B_{y_\alpha}^{**} S_M - B_x v_\alpha^{**} \\ B_{z_\alpha}^{**} S_M - B_x w_\alpha^{**} \end{pmatrix} = S_\alpha^* \begin{pmatrix} \rho_\alpha^* v_\alpha^* \\ \rho_\alpha^* w_\alpha^* \\ B_{y_\alpha}^* \\ B_{z_\alpha}^* \end{pmatrix} - \begin{pmatrix} \rho_\alpha^* v_\alpha^* S_M - B_x B_{y_\alpha}^* \\ \rho_\alpha^* w_\alpha^* S_M - B_x B_{z_\alpha}^* \\ B_{y_\alpha}^* S_M - B_x v_\alpha^* \\ B_{z_\alpha}^* S_M - B_x w_\alpha^* \end{pmatrix}, \tag{52}$$

appear not to be solvable if S_α^* is defined by (51).

Therefore, we consider the jump conditions for the tangential components of the velocity and magnetic field across S_M,

$$S_M \begin{pmatrix} \rho_L^* v_L^{**} \\ \rho_L^* w_L^{**} \\ B_{y_L}^{**} \\ B_{z_L}^{**} \end{pmatrix} - \begin{pmatrix} \rho_L^* v_L^{**} S_M - B_x B_{y_L}^{**} \\ \rho_L^* w_L^{**} S_M - B_x B_{z_L}^{**} \\ B_{y_L}^{**} S_M - B_x v_L^{**} \\ B_{z_L}^{**} S_M - B_x w_L^{**} \end{pmatrix} = S_M \begin{pmatrix} \rho_R^* v_R^{**} \\ \rho_R^* w_R^{**} \\ B_{y_R}^{**} \\ B_{z_R}^{**} \end{pmatrix} - \begin{pmatrix} \rho_R^* v_R^{**} S_M - B_x B_{y_R}^{**} \\ \rho_R^* w_R^{**} S_M - B_x B_{z_R}^{**} \\ B_{y_R}^{**} S_M - B_x v_R^{**} \\ B_{z_R}^{**} S_M - B_x w_R^{**} \end{pmatrix}. \tag{53}$$

It is obvious that the equalities

$$v_L^{**} = v_R^{**} \equiv v^{**}, \tag{54}$$

$$w_L^{**} = w_R^{**} \equiv w^{**}, \tag{55}$$

$$B_{y_L}^{**} = B_{y_R}^{**} \equiv B_y^{**}, \tag{56}$$

$$B_{z_L}^{**} = B_{z_R}^{**} \equiv B_z^{**} \tag{57}$$

are derived from (53) if $B_x \neq 0$. These equalities indicate the conditions for the contact discontinuities (5). On the other hand, if $B_x = 0$, (53) also becomes unsolvable. The case of $B_x = 0$ is discussed later. The relations (54)–(57) show that v, w, B_y, and B_z are approximated by three intermediate states in our assumption

(Fig. 4). Therefore, by substituting (49),(51), and (54)–(57) into the integral conservation laws over the Riemann fan,

$$(S_R - S_R^*)\mathbf{U}_R^* + (S_R^* - S_M)\mathbf{U}_R^{**} + (S_M - S_L^*)\mathbf{U}_L^{**} + (S_L^* - S_L)\mathbf{U}_L^* - S_R\mathbf{U}_R + S_L\mathbf{U}_L + \mathbf{F}_R - \mathbf{F}_L = 0, \quad (58)$$

it is derived that

$$v^{**} = \frac{\sqrt{\rho_L^*}v_L^* + \sqrt{\rho_R^*}v_R^* + (B_{y_R}^* - B_{y_L}^*)\mathrm{sign}(B_x)}{\sqrt{\rho_L^*} + \sqrt{\rho_R^*}}, \quad (59)$$

$$w^{**} = \frac{\sqrt{\rho_L^*}w_L^* + \sqrt{\rho_R^*}w_R^* + (B_{z_R}^* - B_{z_L}^*)\mathrm{sign}(B_x)}{\sqrt{\rho_L^*} + \sqrt{\rho_R^*}}, \quad (60)$$

$$B_y^{**} = \frac{\sqrt{\rho_L^*}B_{y_R}^* + \sqrt{\rho_R^*}B_{y_L}^* + \sqrt{\rho_L^*\rho_R^*}(v_R^* - v_L^*)\mathrm{sign}(B_x)}{\sqrt{\rho_L^*} + \sqrt{\rho_R^*}}, \quad (61)$$

$$B_z^{**} = \frac{\sqrt{\rho_L^*}B_{z_R}^* + \sqrt{\rho_R^*}B_{z_L}^* + \sqrt{\rho_L^*\rho_R^*}(w_R^* - w_L^*)\mathrm{sign}(B_x)}{\sqrt{\rho_L^*} + \sqrt{\rho_R^*}}, \quad (62)$$

where $\mathrm{sign}(B_x)$ is 1 for $B_x > 0$ and -1 for $B_x < 0$. Here, it is found that the jump conditions across S_α^* (52) are satisfied by (59)–(62). Finally, the jump condition of the energy density across S_α^* waves can be solved as

$$e_\alpha^{**} = e_\alpha^* \mp \sqrt{\rho_\alpha^*}(\mathbf{v}_\alpha^* \cdot \mathbf{B}_\alpha^* - \mathbf{v}^{**} \cdot \mathbf{B}^{**})\mathrm{sign}(B_x), \quad (63)$$

where the minus and the plus of the right side correspond to $\alpha = \mathrm{L}$ and R, respectively.

In this way, we can derive the complete set of the intermediate states, $\mathbf{U}_L^*, \mathbf{U}_L^{**}, \mathbf{U}_R^{**}$, and $\mathbf{U}_R^*$, and corresponding fluxes, $\mathbf{F}_L^*, \mathbf{F}_L^{**}, \mathbf{F}_R^{**}$ and $\mathbf{F}_R^*$, which are satisfied with all jump conditions in our approximate Riemann problem. Therefore, the numerical fluxes of our solver are obtained by the integral of conservation laws over the left or the right half of the Riemann fan, $(S_L\Delta t, 0) \times (0, \Delta t)$ or $(0, S_R\Delta t) \times (0, \Delta t)$, as in (8), for instance such that

$$\mathbf{F} = \mathbf{F}_L + S_L\mathbf{U}_L^* - S_L\mathbf{U}_L = \mathbf{F}_L^* \quad (64)$$

for $S_L \leqslant 0 \leqslant S_L^*$, or

$$\mathbf{F} = \mathbf{F}_L + S_L^*\mathbf{U}_L^{**} - (S_L^* - S_L)\mathbf{U}_L^* - S_L\mathbf{U}_L = \mathbf{F}_L^{**} \quad (65)$$

for $S_L^* \leqslant 0 \leqslant S_M$. In general, the fluxes are given by

$$\mathbf{F}_{\mathrm{HLLD}} = \begin{cases} \mathbf{F}_L & \text{if } S_L > 0, \\ \mathbf{F}_L^* & \text{if } S_L \leqslant 0 \leqslant S_L^*, \\ \mathbf{F}_L^{**} & \text{if } S_L^* \leqslant 0 \leqslant S_M, \\ \mathbf{F}_R^{**} & \text{if } S_M \leqslant 0 \leqslant S_R^*, \\ \mathbf{F}_R^* & \text{if } S_R^* \leqslant 0 \leqslant S_R, \\ \mathbf{F}_R & \text{if } S_R < 0. \end{cases} \quad (66)$$

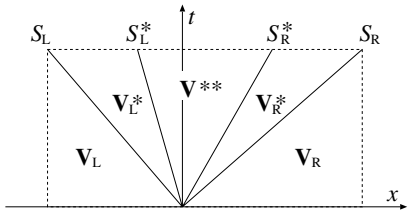

Fig. 4. Schematic structure of the Riemann fan with three intermediate states.

This solver is named as HLLD solver because, as shown in the next subsection, not only isolated contact discontinuities but also isolated all other discontinuities (not shocks) in the MHD system are exactly resolved, i.e., "D" represents all Discontinuities in MHD.

It is found at once that the four-state HLL Riemann solver for MHD as illustrated in Fig. 3 is naturally reduced to the two-state solver as in Fig. 2 for $B_x = 0$ because, in this case, $S_L^* = S_R^* = S_M$ from (51). Therefore, the estimation of the inner intermediate states as (59)–(62) is not necessary for the case of $B_x = 0$. Note also that the HLLC solver for the Euler equations [2,29] is included in the HLLD solver for the MHD equations as the limit of zero magnetic field.

In order to obtain the exact upper and lower bounds of the signal speeds for the Riemann problem, complicated exact solutions for the MHD Riemann problem are needed [2]. Therefore, S_L and S_R may be estimated approximately by (12) or (13). Also, since the explicit expressions of the largest and smallest eigenvalues for MHD are known as in (3), other estimations may be utilized, for instance such that

$$S_L = \min(u_L, u_R) - \max(c_{fL}, c_{fR}), \quad S_R = \max(u_L, u_R) + \max(c_{fL}, c_{fR}), \tag{67}$$

or any adequate estimations (e.g., [16]).

5.2. Exact resolution of isolated discontinuities and shocks

At an isolated tangential discontinuity (6),

$$u_L = u_R = u, \quad p_{T_L} = p_{T_R} = p_T. \tag{68}$$

Substituting (68) into (38) gives

$$S_M = \frac{(S_R - u)\rho_R u - (S_L - u)\rho_L u}{(S_R - u)\rho_R - (S_L - u)\rho_L} = u. \tag{69}$$

Then, by substituting (69) into (43) to (48), it is obtained that

$$\mathbf{U}_L^* = \mathbf{U}_L, \quad \mathbf{U}_R^* = \mathbf{U}_R. \tag{70}$$

In the case of which tangential discontinuities can be formed, i.e., $B_x = 0$, the HLLD solver is reduced to the two-state HLL solver as stated previously. Thus, the HLLD solver gives the exact solution of an isolated tangential discontinuity for a general x/t,

$$\mathbf{U} = \begin{cases} \mathbf{U}_L & \text{if } x/t < u, \\ \mathbf{U}_R & \text{if } x/t > u. \end{cases} \tag{71}$$

At an isolated contact discontinuity (5), in addition to (68),

$$v_L = v_R = v, \quad w_L = w_R = w, \quad B_{y_L} = B_{y_R} = B_y, \quad B_{z_L} = B_{z_R} = B_z. \tag{72}$$

From the condition (68), (70) is obtained in the same way. Also, by substituting (72) into (59)–(63) with (49),

$$\mathbf{U}_L^{**} = \mathbf{U}_L, \quad \mathbf{U}_R^{**} = \mathbf{U}_R. \tag{73}$$

Therefore, an isolated contact discontinuity can be resolved exactly as (71) in the HLLD solver.

Rotational discontinuities must satisfy the jump conditions of (4). Therefore, at an isolated rotational discontinuity,

$$\rho_L = \rho_R = \rho, \tag{74}$$

besides (68). Therefore, the wave speed of an isolated rotational discontinuity is given by

$$s_A = u \pm \frac{|B_x|}{\sqrt{\rho}}, \tag{75}$$

that is, $s_A = \lambda_2$ or λ_6 of (3). Without loss of generality, assume here that $B_x > 0$ and $s_A > u$. In this case, the relations,

$$\sqrt{\rho}(v_R - v_L) = -\left(B_{y_R} - B_{y_L}\right), \quad \sqrt{\rho}(w_R - w_L) = -(B_{z_R} - B_{z_L}), \tag{76}$$

must be realized from the jump conditions. Similar to the discussion for an isolated contact or tangential discontinuity, (70) is obtained from (68). Substituting (76) into (59)–(63) gives

$$\mathbf{U}_L^{**} = \mathbf{U}_R^{**} = \mathbf{U}_L \tag{77}$$

with the help of

$$e_R - e_L = -\sqrt{\rho}(\mathbf{v}_R \cdot \mathbf{B}_R - \mathbf{v}_L \cdot \mathbf{B}_L). \tag{78}$$

The equalities (77) are retained also for $B_x < 0$. On the other hand, when $s_A < u$,

$$\mathbf{U}_L^{*} = \mathbf{U}_L, \quad \mathbf{U}_L^{**} = \mathbf{U}_R^{**} = \mathbf{U}_R^{*} = \mathbf{U}_R. \tag{79}$$

Therefore, in general,

$$\mathbf{U} = \begin{cases} \mathbf{U}_L & \text{if } x/t < s_A, \\ \mathbf{U}_R & \text{if } x/t > s_A. \end{cases} \tag{80}$$

Thus it is shown that the HLLD solver also resolves an isolated rotational discontinuity exactly.

The speed of an isolated fast shock s_f is computed as the largest or smallest eigenvalue of the Roe matrix. We may consider an isolated shock corresponding to the largest eigenvalue only, i.e., $s_f = \lambda_7^{\mathrm{Roe}}$, because of the symmetry of the left and the right states. The left and the right states at an isolated fast shock are related by

$$s_f(\mathbf{U}_R - \mathbf{U}_L) = \mathbf{F}_R - \mathbf{F}_L. \tag{81}$$

Once the maximum signal speed S_R in the HLLD solver is given by the exact shock velocity, (38) gives

$$S_M = \frac{(s_f - u_L)\rho_L u_L - (S_L - u_L)\rho_L u_L}{(s_f - u_L)\rho_L - (S_L - u_L)\rho_L} = u_L \tag{82}$$

by using the jump conditions for the continuity equation and the normal component of the momentum equation in (81). Also,

$$p_T^{*} = p_{T_L}, \tag{83}$$

by substituting (82) into (41) or equivalently (23). Then, substituting (82) and (83) into (43)–(48), some algebraic manipulations with the help of (81) give

$$\mathbf{U}_L^{*} = \mathbf{U}_R^{*} = \mathbf{U}_L. \tag{84}$$

Therefore, it is also obtained straightforwardly from (59)–(63) that

$$\mathbf{U}_L^{**} = \mathbf{U}_R^{**} = \mathbf{U}_L. \tag{85}$$

Similarly, when $s_f = S_L$,

$$\mathbf{U}_L^{*} = \mathbf{U}_L^{**} = \mathbf{U}_R^{**} = \mathbf{U}_R^{*} = \mathbf{U}_R. \tag{86}$$

Thus, the exact shock solution,

$$\mathbf{U} = \begin{cases} \mathbf{U}_L & \text{if } x/t < s_f, \\ \mathbf{U}_R & \text{if } x/t > s_f, \end{cases} \tag{87}$$

is obtained in the HLLD solver. It is noted that the exact resolution of an isolated fast shock (87) relies on the proper choices of S_L and S_R, and thus, the algorithm of (13) is appropriate in this particular viewpoint. On the other hand, the resolution of an isolated contact, tangential discontinuity (71) and rotational discontinuity (80) does not depend on the detailed estimation of S_R and S_L.

5.3. Positivity of HLLD solver

Consider the set of the physically realistic states with positive densities and positive pressures for the MHD equations such that

$$G = \left\{ \begin{bmatrix} \rho \\ \rho u \\ \rho v \\ \rho w \\ B_y \\ B_z \\ e \end{bmatrix}, \rho > 0 \text{ and } e - \frac{1}{2}\rho|\mathbf{v}|^2 - \frac{1}{2}|\mathbf{B}|^2 > 0 \right\}.$$

In the MHD equations, and likewise in the Euler equations, the average states defined by $\mathbf{U} = (1-\theta)\mathbf{U}_1 + \theta\mathbf{U}_2$ with $0 \leqslant \theta \leqslant 1$ are physically realistic states if both $\mathbf{U}_1$ and $\mathbf{U}_2$ are physical [16]. Since Godunov-type schemes update the subsequent states by averaging the states of the exact or the approximate solution of the Riemann problem, a positively conservative scheme can be constructed in those schemes if all the states generated are physical. Thus, a positively conservative Riemann solver generates states in G if the preceding states are contained in G.

We now consider the right outer and inner intermediate states, $\mathbf{U}_R^*$ and $\mathbf{U}_R^{**}$. The positivity preserving conditions become

$$\rho_R^* > 0, \tag{88}$$

$$\rho_R^{**} > 0, \tag{89}$$

$$p_R^* = (\gamma-1)\left(e_R^* - \frac{1}{2}\rho_R^*|\mathbf{v}_R^*|^2 - \frac{1}{2}|\mathbf{B}_R^*|^2\right) > 0, \tag{90}$$

$$p_R^{**} = (\gamma-1)\left(e_R^{**} - \frac{1}{2}\rho_R^{**}|\mathbf{v}_R^{**}|^2 - \frac{1}{2}|\mathbf{B}_R^{**}|^2\right) > 0. \tag{91}$$

In order to simplify the subsequent arguments, the following variables are introduced:

$$\xi \equiv S_R - u_R, \quad \eta \equiv S_R - S_M, \quad \zeta \equiv S_M - u_R. \tag{92}$$

Since S_R is the maximum signal speed in the Riemann system, both ξ and η are positive. On the other hand, ζ can be either positive or negative.

The conditions of (88) and (89) are easily shown from (43) and (49) such that

$$\rho_R^* = \rho_R^{**} = \frac{\xi}{\eta}\rho_R > 0. \tag{93}$$

To show the inequality (90), let us consider the positivity of φ defined and rearranged by some algebraic manipulations as follows:

$$\begin{aligned}\varphi &\equiv \eta\left(e^*_{\mathrm{R}} - \frac{1}{2}\rho^*_{\mathrm{R}}|\mathbf{v}^*_{\mathrm{R}}|^2 - \frac{1}{2}|\mathbf{B}^*_{\mathrm{R}}|^2\right)\\ &= \frac{\rho_{\mathrm{R}}\xi}{2}\zeta^2 + p_{\mathrm{R}}\zeta + \frac{p_{\mathrm{R}}\xi}{\gamma-1} + \frac{\rho_{\mathrm{R}}\xi}{2}(|\mathbf{v}_{\perp_{\mathrm{R}}}|^2 - |\mathbf{v}^*_{\perp_{\mathrm{R}}}|^2) + \frac{\xi}{2}(|\mathbf{B}_{\perp_{\mathrm{R}}}|^2 - |\mathbf{B}^*_{\perp_{\mathrm{R}}}|^2) + \frac{\zeta}{2}(|\mathbf{B}_{\perp_{\mathrm{R}}}|^2 + |\mathbf{B}^*_{\perp_{\mathrm{R}}}|^2)\\ &\quad + B_x(\mathbf{v}_{\perp_{\mathrm{R}}}\cdot\mathbf{B}_{\perp_{\mathrm{R}}} - \mathbf{v}^*_{\perp_{\mathrm{R}}}\cdot\mathbf{B}^*_{\perp_{\mathrm{R}}})\\ &= \frac{\rho_{\mathrm{R}}\xi}{2}\left(1 - \frac{|\mathbf{B}_{\perp_{\mathrm{R}}}|^2}{\rho_{\mathrm{R}}\xi\eta - B_x^2}\right)\zeta^2 + p_{\mathrm{R}}\zeta + \frac{p_{\mathrm{R}}\xi}{\gamma-1},\end{aligned} \tag{94}$$

where $\mathbf{v}_\perp = (0, v, w)$ and $\mathbf{B}_\perp = (0, B_y, B_z)$. It is noted that (94) is identical to the corresponding equation for the HLLC solver [2] except for the correction in the first term. Since S_{R} is expressed by λ_7 of (3) and is the maximum speed in the Riemann system, the inequalities, $\xi \geqslant c_{\mathrm{f}_{\mathrm{R}}}$ and $\eta \geqslant c_{\mathrm{f}_{\mathrm{R}}}$, will be satisfied. Therefore,

$$\varphi' = \frac{\rho_{\mathrm{R}}\xi}{2}\left(1 - \frac{|\mathbf{B}_{\perp\mathrm{R}}|^2}{\rho_{\mathrm{R}}c^2_{\mathrm{f}_{\mathrm{R}}} - B_x^2}\right)\zeta^2 + p_{\mathrm{R}}\zeta + \frac{p_{\mathrm{R}}\xi}{\gamma-1} \leqslant \varphi. \tag{95}$$

This relation indicates that φ is necessarily positive if φ' is positive. (We point out here that Gurski [13] misled a "stronger condition" for positivity in view of the inequality (95).) Since $\rho c_{\mathrm{f}}^2 - |\mathbf{B}|^2 = \rho c_{\mathrm{f}}^2 - B_x^2 - |\mathbf{B}_\perp|^2 > 0$ except when $\mathbf{B}_\perp = 0$ and $B_x^2 \geqslant \gamma p$, the first term of (95) is necessarily positive. Note that φ in the case of $\mathbf{B}_\perp = 0$ fully corresponds to that for the HLLC solver [2], and therefore, the positivity of φ is assured in this case. Thus, since all coefficients with respect to ζ are positive, φ' is positive for any ζ if the discriminant of φ' is negative:

$$D(\varphi') = p_{\mathrm{R}}^2 - \frac{2\rho_{\mathrm{R}}p_{\mathrm{R}}}{\gamma-1}\left(1 - \frac{|\mathbf{B}_{\perp_{\mathrm{R}}}|^2}{\rho_{\mathrm{R}}c^2_{\mathrm{f}_{\mathrm{R}}} - B_x^2}\right)\xi^2 < 0.$$

Therefore,

$$\xi^2 > \frac{(\gamma-1)p_{\mathrm{R}}}{2\rho_{\mathrm{R}}}\left(1 - \frac{|\mathbf{B}_{\perp_{\mathrm{R}}}|^2}{\rho_{\mathrm{R}}c^2_{\mathrm{f}_{\mathrm{R}}} - B_x^2}\right)^{-1}. \tag{96}$$

If $B_x \neq 0$, by using the relations that

$$\rho c_{\mathrm{s}}^2 - B_x^2 = -\frac{B_x^2|\mathbf{B}_\perp|^2}{\rho c_{\mathrm{f}}^2 - B_x^2}, \quad c_{\mathrm{f}}^2 c_{\mathrm{s}}^2 = \frac{\gamma p B_x^2}{\rho^2},$$

(96) can be rewritten as

$$\xi^2 > \frac{\gamma-1}{2\gamma}c^2_{\mathrm{f}_{\mathrm{R}}}. \tag{97}$$

Also, if $B_x = 0$, where $\rho c_{\mathrm{f}}^2 = \gamma p + |\mathbf{B}_\perp|^2$, the identical inequality is easily derived from (96). Therefore, from (92) and (97), in order to preserve the positivity of the pressure (90), S_{R} must be chosen to be satisfied with the inequality as

$$S_{\mathrm{R}} > u_{\mathrm{R}} + \sqrt{\frac{\gamma-1}{2\gamma}}c_{\mathrm{f}_{\mathrm{R}}}. \tag{98}$$

Note that the resultant inequality (98) is quite similar to the corresponding inequality for the HLLC solver (22) but the fast magnetosonic speed $c_{\mathrm{f}_{\mathrm{R}}}$ must be replaced by the sound speed a_{R}. As found form (12), (13),

or (67), since the HLLD solver for MHD clearly satisfies (98), our solver ensures the positivity preserving property (90).

Subsequently, if the pressure at the outer states is retained as positive, the positivity of the pressure at the inner states is shown straightforwardly by using (59)–(63) to be

$$\begin{aligned} p_{\mathrm{R}}^{**} &= (\gamma-1)\left(e_{\mathrm{R}}^{**} - \frac{1}{2}\rho_{\mathrm{R}}^{*}|\mathbf{v}^{**}|^2 - \frac{1}{2}|\mathbf{B}^{**}|^2\right) \\ &= p_{\mathrm{R}}^{*} + \frac{\gamma-1}{2}\left(\left|\sqrt{\rho_{\mathrm{R}}^{*}}\mathbf{v}_{\mathrm{R}}^{*} + \mathbf{B}_{\mathrm{R}}^{*}\mathrm{sign}(B_x)\right|^2 - \left|\sqrt{\rho_{\mathrm{R}}^{*}}\mathbf{v}^{**} + \mathbf{B}^{**}\mathrm{sign}(B_x)\right|^2\right) = p_{\mathrm{R}}^{*} > 0. \end{aligned} \tag{99}$$

Also, it is noted from (99) that our solver is consistent with the continuous condition of the pressure across rotational discontinuities.

The positivity of the density and pressure at the left outer and inner intermediate states, $\mathbf{U}_{\mathrm{L}}^{*}$ and $\mathbf{U}_{\mathrm{L}}^{**}$, is also assured if the inequality,

$$S_{\mathrm{L}} < u_{\mathrm{L}} - \sqrt{\frac{\gamma-1}{2\gamma}}c_{\mathrm{f_L}}, \tag{100}$$

is satisfied. Thus, the proof of the positivity is completed. It is obvious that (98) and (100) are stronger than the conditions by Gurski [13]. The present proof will also be applicable to the single-state HLL Riemann solver since the one intermediate state of the HLL solver is given by the average of the HLLD intermediate states contained in G.

At the end of this subsection, we reconsider the prerequisite inequalities to obtain a stronger condition for the pressure positivity (95). We find at once that the prerequisite inequality as $\xi \geqslant c_{\mathrm{f_R}}$ is assured due to the estimation (67) or something equivalent. On the other hand, it is not so easy to confirm whether the other inequality $\eta \geqslant c_{\mathrm{f_R}}$ is satisfied or not at any situation, because S_M is evaluated not only from the right states but also from the left states. In order to simplify the discussion, we only pay attention to expansion waves which are more problematic than shocks in terms of positivity. From the jump condition of the normal momentum across S_{R}, we obtain that

$$\eta = \xi + \frac{p_{\mathrm{T_R}} - p_{\mathrm{T}}^{*}}{\rho_{\mathrm{R}}\xi}.$$

Since $p_{\mathrm{T_R}}$ is greater than p_{T}^{*} under the condition $u_{\mathrm{R}} - u_{\mathrm{L}} > (p_{\mathrm{T_R}} - p_{\mathrm{T_L}})/\rho_{\mathrm{L}}(S_{\mathrm{L}} - u_{\mathrm{L}})$, the inequalities $\eta > \xi \geqslant c_{\mathrm{f_R}}$ are satisfied at such strong expansion waves. Thus, both prerequisite inequalities for the pressure positivity are satisfied in the most problematic situation. Notice that this fact does not mean that other situations than strong expansion waves would necessarily break the prerequisite inequalities. Moreover, since the positivity preserving condition (98) is a rather weak and easily conquerable restriction, the HLLD solver is thought to be a positively conservative scheme.

6. Numerical tests

We present in this section results for several test problems computed by the HLLD Riemann solver. For comparison, the same problems are solved by the single-state HLL Riemann solver and the standard linearized Riemann solver, the so-called Roe scheme [26], in which we adopt the Roe average by Balsara [1]. Also, the HLLD solver is compared with the variants of the HLLC-type solver. In our tests, as an algorithm to estimate S_{L} and S_{R}, (67) is used for simplicity and efficiency because numerical solutions by (67) are indistinguishable from those by (13) in spite of not resolving isolate fast shocks exactly. Also, γ is fixed to 5/3 throughout our numerical tests. In order to evaluate the essential abilities of the solver,

we restrict our attention to the scheme of first-order accuracy in space and second-order in time without additional notice.

6.1. One-dimensional shock tube problems

We perform several one-dimensional shock tube problems which are solved within the interval $-0.5 \leqslant x \leqslant 0.5$, with 800 grid points, and with a CFL number of 0.8, through this subsection.

We perform a typical shock tube problem presented first by Dai and Woodward [6], and tested by Ryu and Jones [27] and many others, where the initial states are given by $(\rho, p, u, v, w, B_y, B_z) = (1.08, 0.95, 1.2, 0.01, 0.5, 3.6/\sqrt{4\pi}, 2/\sqrt{4\pi})$ for $x < 0$, $(1, 1, 0, 0, 0, 4/\sqrt{4\pi}, 2/\sqrt{4\pi})$ for $x > 0$, with $B_x = 4/\sqrt{4\pi}$. The exact solution of this problem is composed of various shocks and discontinuities; two fast shocks, two rotational discontinuities, two slow shocks, one contact discontinuity [6,27]. In Fig. 5, the numerical results are plotted at $t = 0.2$. It is found that the numerical solution of the HLLD solver seems to be indistinguishable from that of the Roe scheme, whereas the HLL solver cannot resolve the contact and the rotational discontinuities in particular. The magnifications of the density profile, where the solution of the HLL solver is omitted for clarity, around the fast and slow shocks at the left of the contact discontinuity also indicate that the resolution of the HLLD solver is almost equal to that of the Roe scheme even for the slow shock in this problem.

Since the solution of this problem includes all ordinary discontinuities in MHD, it is worth considering whether the similar solvers to the HLLD solver, the variants of the HLLC-type solver by Gurski (HLLC-G) [13] and by Li (HLLC-L) [19], can resolve discontinuities and shocks well or not. While the smooth HLLC-type solver [13] was thought to be comparable with one of the Linde solver [20], another Linde's solver [21] seemed to be less accurate than the HLLC-L solver [19]. Thus, the numerical test by the smooth HLLC-type solver are not performed. Since all solvers tested here may resolve isolated fast shocks exactly if we choose (13), the resolution of the fast shocks in these solvers seems to be comparable with one another. In order to be clear about the differences of the solvers, we only show the solution without the fast shocks in Fig. 6. The difference between the results of the HLLD solver and that of the Roe scheme is invisible even in this enlarged figure. We find that the HLLC-type solvers as well as the HLLD solver can resolve the contact discontinuity as expected although the contact discontinuity is smeared out by the HLL solver. The rotational discontinuities, on the other hand, are extremely smeared out in both of the HLLC-type solvers although the HLLC-L solver is slightly more accurate in comparison with the HLLC-G solver. As a consequence, the numerical solution of the HLL or the HLLC-type solver seems to be quite different from the solution of the HLLD solver or the Roe scheme. We also find from Fig. 7 that the resolution of the HLLC-type solver cannot be recovered to the level of the HLLD solver or the Roe scheme even when the solvers are extended to second-order accuracy in space, which are achieved by a linear reconstruction for the primitive variables with minmod limiter. The failure of the HLLC-type solvers is probably caused by the assumption that the magnetic field is constant over the Riemann fan. Thus, the HLLD solver has an obvious advantage over the two-state Riemann solvers.

We also test a standard shock tube problem first discussed by Brio and Wu [4] and tested by many others, where the initial states are $(\rho, p, u, v, w, B_y, B_z) = (1, 1, 0, 0, 0, 1, 0)$ for $x < 0$, $(0.125, 0.1, 0, 0, 0, -1, 0)$ for $x > 0$, with $B_x = 0.75$. Although $\gamma = 2$ in the original test, our test follows the corresponding test by Ryu and Jones [27] with $\gamma = 5/3$. Fig. 8 shows the results at $t = 0.1$, which include not only ordinary waves but also the slow compound wave caused by the non-convexity of the MHD equations. We find that the numerical solution of the HLLD solver is almost comparable to that of the Roe scheme as a whole, whereas the contact and compound waves are not well resolved by the single-state HLL solver. The magnifications of the density around the slow compound wave and the slow shock, however, indicate that the solution of the HLLD solver seems to be slightly smeared out compared with that of the Roe scheme although the peaks of the density on the compound wave are little different from each other ($\rho^{\mathrm{Roe}} = 0.820$, $\rho^{\mathrm{HLLD}} = 0.815$), and

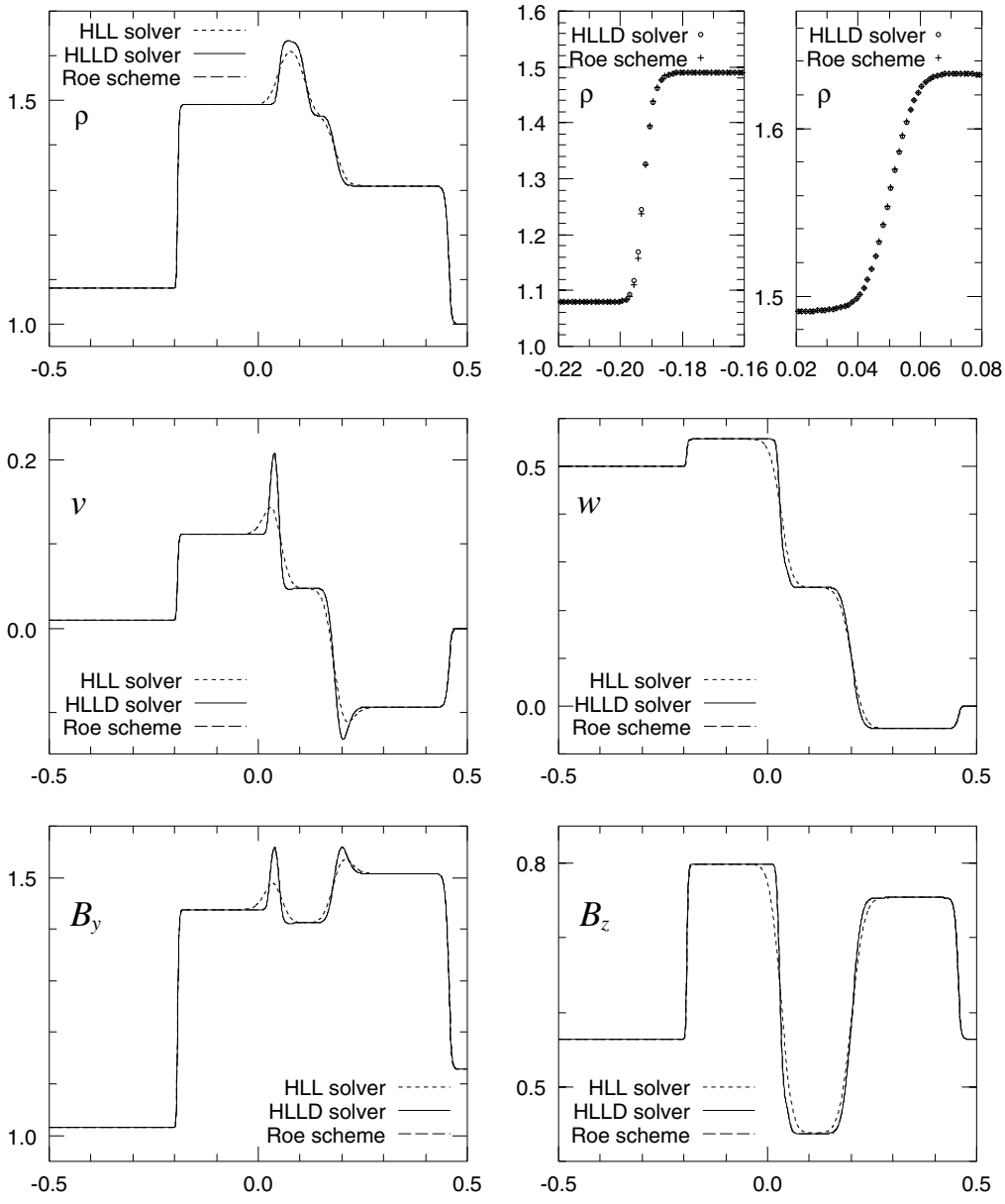

Fig. 5. Results of one-dimensional shock tube test with the initial left states $(\rho, p, u, v, w, B_y, B_z) = (1.08, 0.95, 1.2, 0.01, 0.5, 3.6/\sqrt{4\pi}, 2/\sqrt{4\pi})$, the right states $(1, 1, 0, 0, 0, 4/\sqrt{4\pi}, 2/\sqrt{4\pi})$, and $B_x = 4/\sqrt{4\pi}$. Numerical solutions of the HLL solver, the HLLD solver, and the Roe scheme are plotted at $t = 0.2$. (Top left) ρ, (middle left) v, (middle right) w, (bottom left) B_y, (bottom right) B_z, (top middle) ρ around the left fast shock, (top right) ρ around the left slow shock are shown.

the differences may not be important. The smaller resolution of the slow shocks in the HLLD solver may be because the slow waves in the Riemann fan are not explicitly included. On the other hand, although the solution near the head of the rarefaction attached to the compound wave are almost equivalent, the tail of the compound rarefaction calculated by our Roe scheme seems to be very slightly undershot. This fact

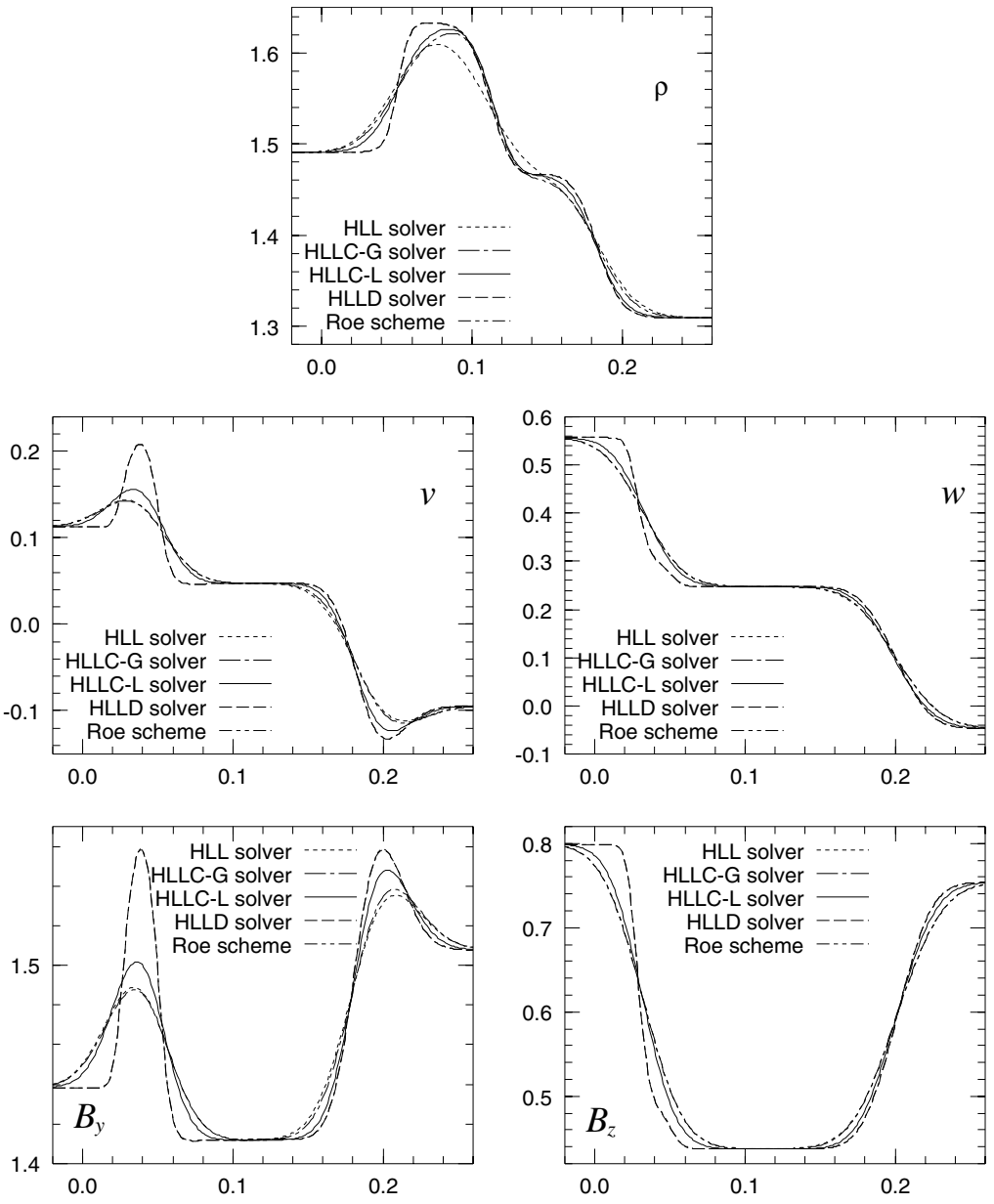

Fig. 6. Results of one-dimensional shock tube test with the same initial states as in Fig. 5. Numerical solutions of the HLL solver, the HLLC-type solver by Gurski (HLLC-G) [13], the HLLC-type solver by Li (HLLC-L) [19], the HLLD solver, the Roe scheme are plotted at $t = 0.2$. (Top) ρ, (middle left) v, (middle right) w, (bottom left) B_y, (bottom right) B_z are shown within $-0.02 < x < 0.26$.

might be due to the underestimation of the signal speed of the rarefaction wave in the Roe scheme, which is inevitable for the linearized Riemann solver. Corresponding undershoots are not observed in the HLLD solver.

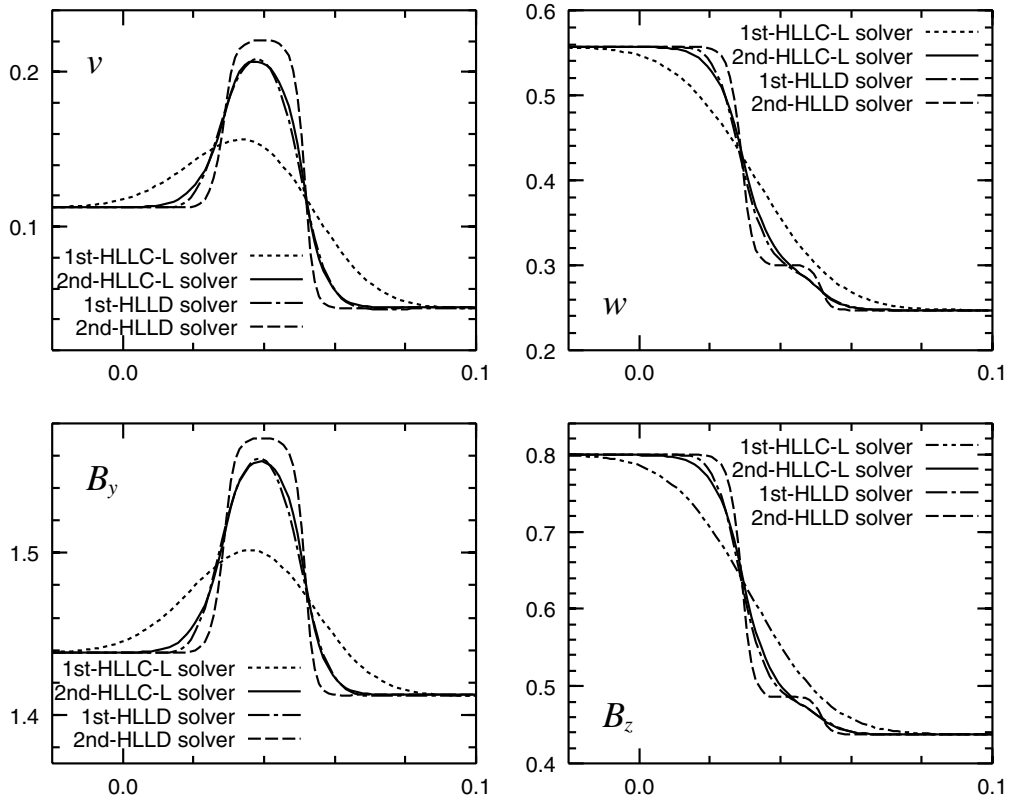

Fig. 7. Results of one-dimensional shock tube test with the same initial states as in Fig. 5. Numerical solutions of the first- and second-order HLLC-type solver by Li (1st- and 2nd-HLLC-L) [19], the first- and second-order HLLD solver (1st- and 2nd-HLLD) are plotted at $t = 0.2$. (Top left) v, (top right) w, (bottom left) B_y, (bottom right) B_z are shown within $-0.02 < x < 0.1$.

Although the above two tests contain a number of different waves and are quite useful when comparing MHD solvers with one another, tests for isolated waves are also meaningful. Since information of the slow waves is lost when constructing the HLLD solver, we concentrate on test problems for the slow waves in particular. Following the test of a slow switch-off shock by Falle et al. [11], the initial states are given by $(\rho, p, u, v, w, B_y, B_z) = (1.368, 1.769, 0.269, 1, 0, 0, 0)$ for $x < 0$, $(1, 1, 0, 0, 0, 1, 0)$ for $x > 0$, with $B_x = 1$. Fig. 9 shows the results at $t = 0.2$, where the tangential component of the magnetic field, B_y, is switched off behind the shock. It is found that the HLLD solver can resolve the isolated slow shock equally to the Roe scheme despite the loss of information on the slow waves while the HLL solver cannot resolve the shock well. We note that an error caused by the jump of the initial states is observed in every solver. We also perform the test of a slow switch-off rarefaction given also by [11], where the initial states are $(\rho, p, u, v, w, B_y, B_z) = (1, 2, 0, 0, 0, 0, 0)$ for $x < 0$, $(0.2, 0.1368, 1.186, 2.967, 0, 1.6405, 0,)$ for $x > 0$, with $B_x = 1$. Fig. 10 shows the results at $t = 0.2$, where B_y is switched off over the head of the rarefaction. Also in this test, a startup error is observed near the tail of the rarefaction. It is thought that such errors may be inevitable unless the initial left and right states are connected continuously with a finite width. We find that the strong slow rarefaction can be calculated by the HLL and the HLLD solvers without any extra numerical dissipation. The isolated fast rarefaction [11] can also be calculated although the results are not shown in this paper. The success of these solvers may be because the solvers are bounded by the maximum and

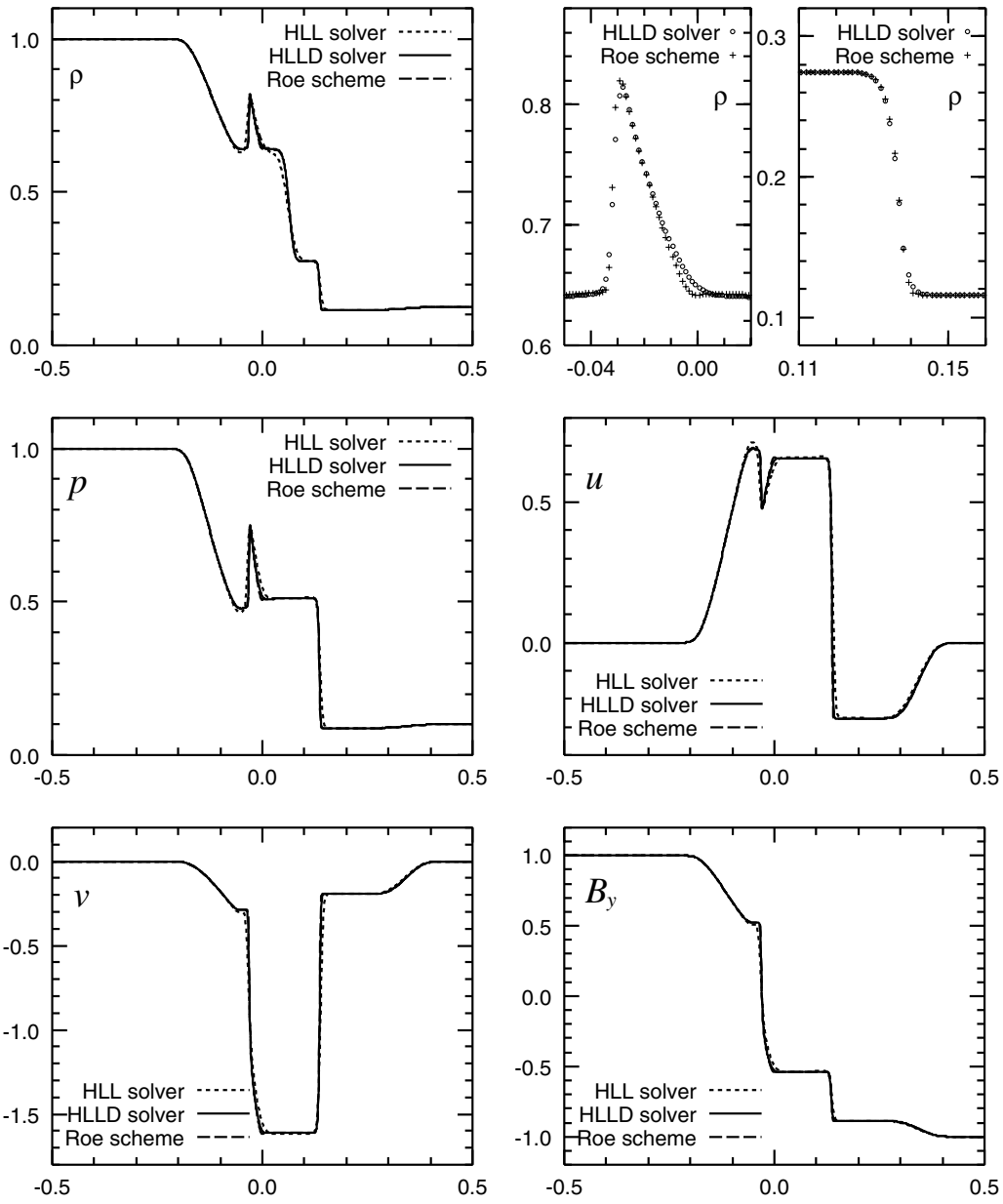

Fig. 8. Results of one-dimensional shock tube test with the initial left states (ρ, p, u, v, w, B_y, B_z) = (1, 1, 0, 0, 0, 1, 0), the right states (0.125, 0.1, 0, 0, 0, −1, 0), and $B_x = 0.75$. Numerical solutions of the HLL solver, the HLLD solver, and the Roe scheme are plotted at $t = 0.1$. (Top left) ρ, (middle left) p, (middle right) u, (bottom left) v, (bottom right) B_y, (top middle) ρ around the slow compound wave, (top right) ρ around the slow shock are shown.

minimum signal speeds in the Riemann fan and, as a result, include the effect of not only the slow rarefaction but also the fast rarefaction properly. On the other hand, the Roe scheme fails in this test, where the entropy condition is broken at $x = 0$. It is found, however, that an additional entropy correction (e.g., [14]) can cure the unphysical solution in this problem.

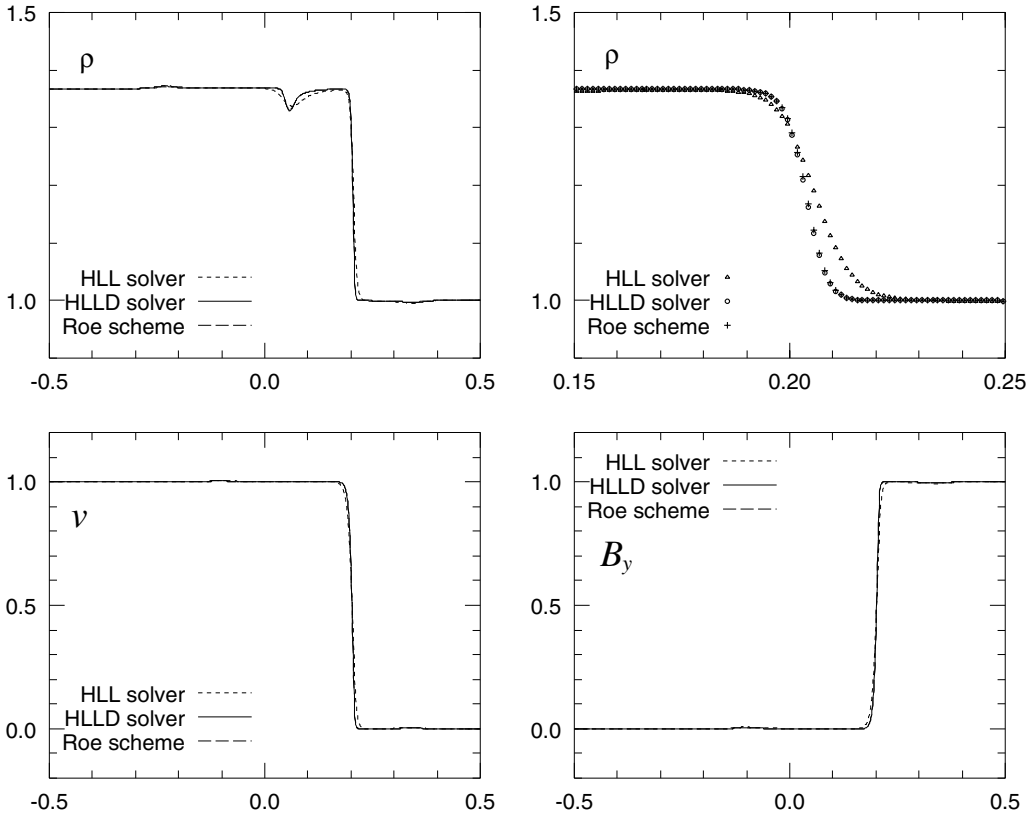

Fig. 9. Results of one-dimensional shock tube test with the initial left states $(\rho, p, u, v, w, B_y, B_z) = (1.368, 1.769, 0.269, 1, 0, 0, 0)$, the right states (1, 1, 0, 0, 0, 1, 0), and $B_x = 1$. Numerical solutions of the HLL solver, the HLLD solver, and the Roe scheme are plotted at $t = 0.2$. (Top left) ρ, (bottom left) v, (bottom right) B_y, (top right) ρ around the slow switch-off shock are shown.

In the final shock tube test, we consider super-fast expansions which may be rather extreme situations. The initial states are given by $(\rho, p, u, v, w, B_y, B_z) = (1, 0.45, -u_0, 0, 0, 0.5, 0)$ for $x < 0$, $(1, 0.45, u_0, 0, 0, 0.5, 0)$ for $x > 0$, with $B_x = 0$. The fast magnetosonic Mach number M_f of the expansion wave is given by u_0 since the fast magnetosonic speed c_f is 1 at the initial states. This type of problem for the Euler equations was shown not to be linearizable for certain Mach numbers [9]. This will also be true for the MHD equations. Indeed, as shown in Fig. 11, although the physically realistic solutions, non-negative density and pressure, can be obtained in the problem with $M_f = 3$ for all solvers, the Roe scheme even with the entropy correction fails in the problem with $M_f = 3.1$. On the other hand, the HLL and the HLLD solvers preserve the positivity without any extra numerical dissipation as expected analytically.

6.2. Applicability to multi-dimensions

It is known that the extension of the one-dimensional upwind-type MHD solver to multi-dimensions is not straightforward because the solenoidal condition of the magnetic field is broken numerically. In order to remove the numerical divergence errors, several approaches have been applied to the upwind-type solver and compared with one another (e.g., [8,30]). Although the so-called constrained transport (CT) method by

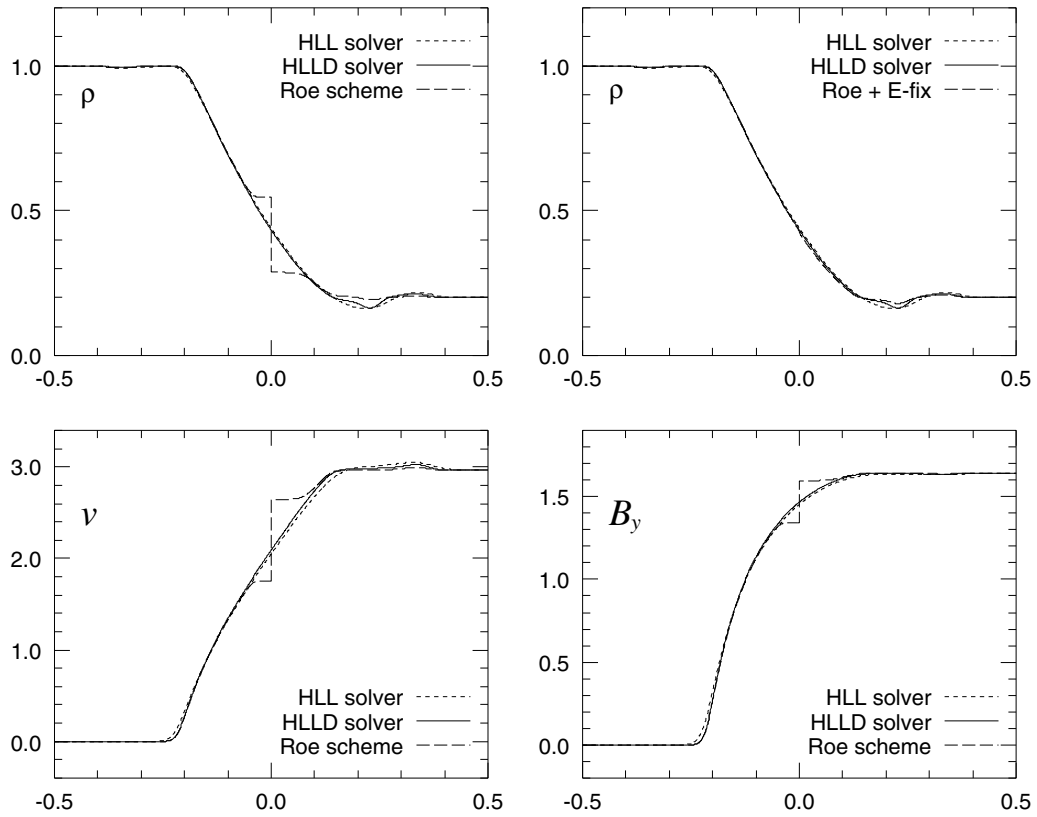

Fig. 10. Results of one-dimensional shock tube test with the initial left states (ρ, p, u, v, w, B_y, B_z) = (1, 2, 0, 0, 0, 0, 0), the right states (0.2, 0.1368, 1.186, 2.967, 0, 1.6405, 0), and $B_x = 1$. Numerical solutions of the HLL solver, the HLLD solver, and the Roe scheme are plotted at $t = 0.2$. (Top left) ρ, (bottom left) v, (bottom right) B_y, (top right) ρ by the Roe scheme with the entropy condition (Roe + E–fix) are shown.

Evans and Hawley [10] can maintain the divergence free condition within machine accuracy, there are no general guidelines to apply any one-dimensional MHD solver properly. Thus, the application of the CT method to the HLLD solver is beyond the scope of this paper. On the other hand, the other divergence cleaning method by projection [3], diffusion [23], or transport [8,25] of divergence errors can be directly added on to existing one-dimensional MHD schemes.

Particularly, Dedner et al. [8] showed that some add-on divergence cleaning methods can be expressed by the so-called generalized Lagrange multiplier (GLM) formulation of the MHD equations. They also pointed out that the choice of the *mixed* hyperbolic/parabolic GLM-MHD gives excellent results since the divergence errors in the mixed GLM-MHD are transported out of the domain by two waves with the maximal admissible speed even in stagnation points and are damped at the same time. The mixed GLM-MHD is also effective in other aspects; easy to implement on an existing code, fast due to the explicit approximation, conservative for the physical quantities. Thus, keeping practical applications in mind, the divergence cleaning method based on the mixed GLM-MHD is adopted in our multi-dimensional test.

We perform, in particular, the so-called Orszag–Tang vortex problem [24] which is a standard two-dimensional test for MHD schemes (e.g., [30] and many other references therein). The Orszag–Tang vortex problem is thought to be appropriate for comparing the resolution of MHD schemes because complex

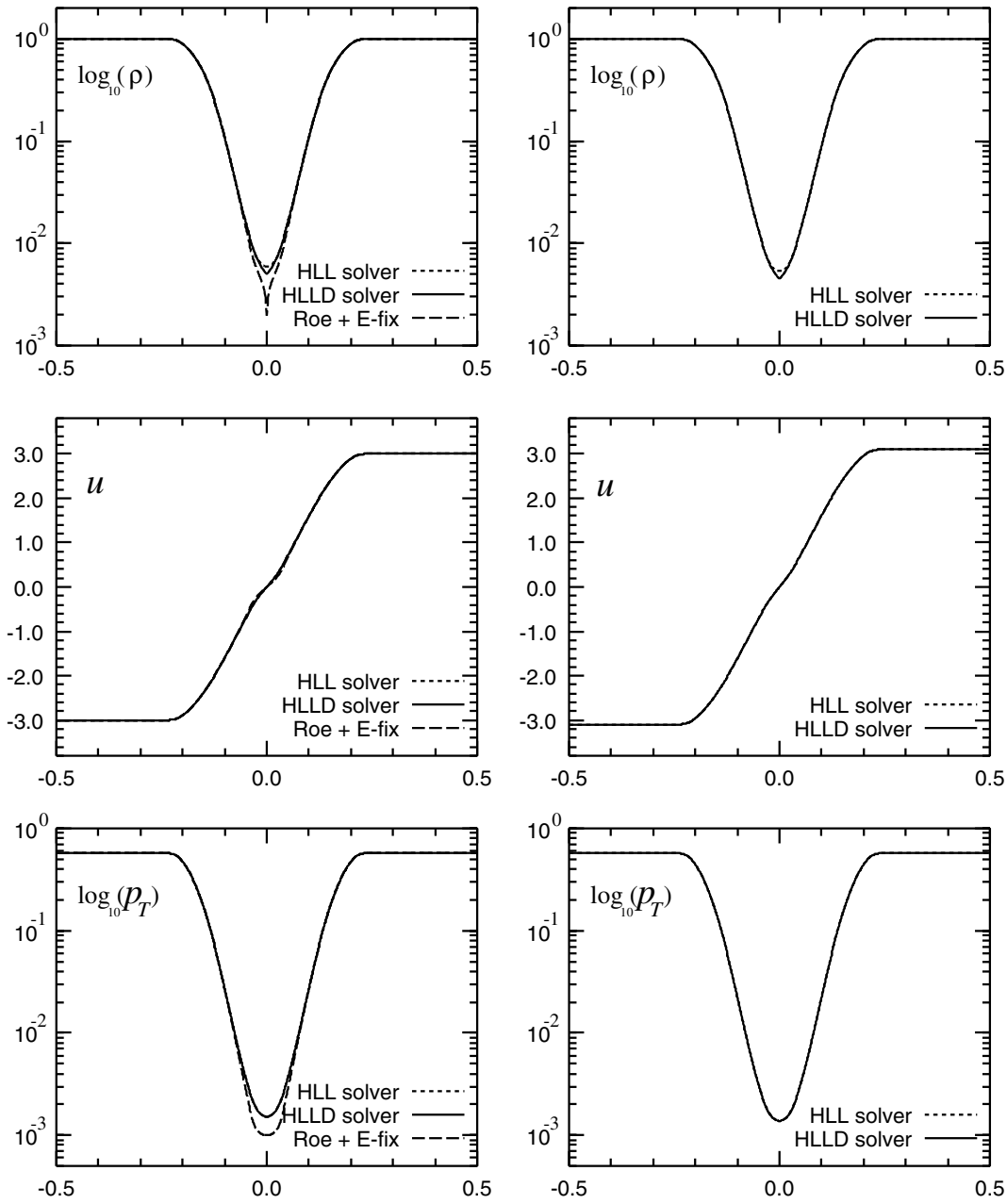

Fig. 11. Results of one-dimensional shock tube test with the initial left states (ρ, p, u, v, w, B_y, B_z) = (1, 0.45, $-u_0$, 0, 0, 0.5, 0), the right states (1, 0.45, u_0, 0, 0, 0.5, 0), and $B_x = 0$. Numerical solutions of the HLL solver, the HLLD solver, and the Roe scheme with the entropy correction (Roe + E–fix) are plotted at $t = 0.05$. (Left) $u_0 = 3$, (right) $u_0 = 3.1$. (Top to bottom) $\log_{10}\rho$, u, $\log_{10}p_T$ are shown. Note that the solution of the Roe scheme is not plotted in the right panel because the Roe scheme fails after several time steps in the case of $u_0 = 3.1$.

Table 1
Relative differences of the temperature from the solution of the Roe scheme with corresponding accuracy and resolution, δT_{Roe}

N	1st HLL	1st HLLD	2nd HLL	2nd HLLD
50	0.0779	0.0054	0.0239	0.0040
100	0.0579	0.0043	0.0143	0.0028
200	0.0453	0.0034	0.0083	0.0027
400	0.0353	0.0024	0.0046	0.0011

interactions of several MHD shock waves are included in the evolution of the vortex. The initial conditions of the problem are given by $(\rho, p, u, v, w, B_x, B_y, B_z) = (\gamma^2, \gamma, -\sin y, \sin x, 0, -\sin y, \sin 2\ x, 0)$ in a square domain $0 < x, y < 2\pi$ with $N \times N$ grids. Periodic boundary conditions are adopted in both coordinate directions. In the present test, second-order accurate schemes with the monotonized central (MC) limiter as well as first-order accurate schemes are compared with one another at the resolution of $N = 50$, 100, 200, and 400. In all simulations, a CFL number of 0.4 is used. Especially, as an indicator of the ability of the schemes, the numerical solution of the temperature $T = p/\rho$ at $t = \pi$ is taken notice of in the following discussions. In Table 1, we show the relative differences of the temperature from the solution of the Roe scheme with corresponding accuracy and grid number defined as

$$\delta T_{\mathrm{Roe}} = \frac{\sum \left| T^{\mathrm{HLL/HLLD}} - T^{\mathrm{Roe}} \right|}{\sum T^{\mathrm{Roe}}},$$

where the summation is taken over the grid cells. We find that δT_{Roe} for the HLL solver becomes large especially with decreasing accuracy and grid number, whereas δT_{Roe} for the HLLD solver is less than 1% in every case. In Table 2, we also summarize the relative differences of the temperature from the reference solution as

$$\delta T_{\mathrm{ref.}} = \frac{\sum \left| T^{\mathrm{HLL/HLLD/Roe}} - T_{\mathrm{ref.}} \right|}{\sum T_{\mathrm{ref.}}},$$

where the reference temperature $T_{\mathrm{ref.}}$ is calculated by the second-order MUSCL Roe scheme with the MC limiter at the finer grid $N = 800$ adopting the projection divergence cleaning method, which is one of the most accurate and reliable method at present [30]. It is found that $\delta T_{\mathrm{ref.}}$ for the HLLD solver is comparable to that for the Roe scheme with corresponding accuracy and resolution within a trivial error although corresponding $\delta T_{\mathrm{ref.}}$ for the HLL solver is large. Indeed, as seen in Figs. 12 and 13, the numerical solution of the HLLD solver is almost equal to that of the Roe scheme over the whole domain, while the HLL solver is less accurate and less resolved than the Roe and HLLD solvers especially around $(x, y) = (\pi, \pi)$. Thus, these results imply that the HLLD MHD solver is applicable to the multi-dimensional problems even with complex wave structures equally to the Roe scheme.

Table 2
Relative differences of the temperature from the reference solution, $\delta T_{\mathrm{ref.}}$

N	1st HLL	1st HLLD	1st Roe	2nd HLL	2nd HLLD	2nd Roe
50	0.4106	0.3661	0.3650	0.1580	0.1365	0.1357
100	0.3340	0.2953	0.2950	0.0844	0.0676	0.0675
200	0.2620	0.2257	0.2257	0.0394	0.0308	0.0315
400	0.1960	0.1644	0.1647	0.0172	0.0132	0.0131

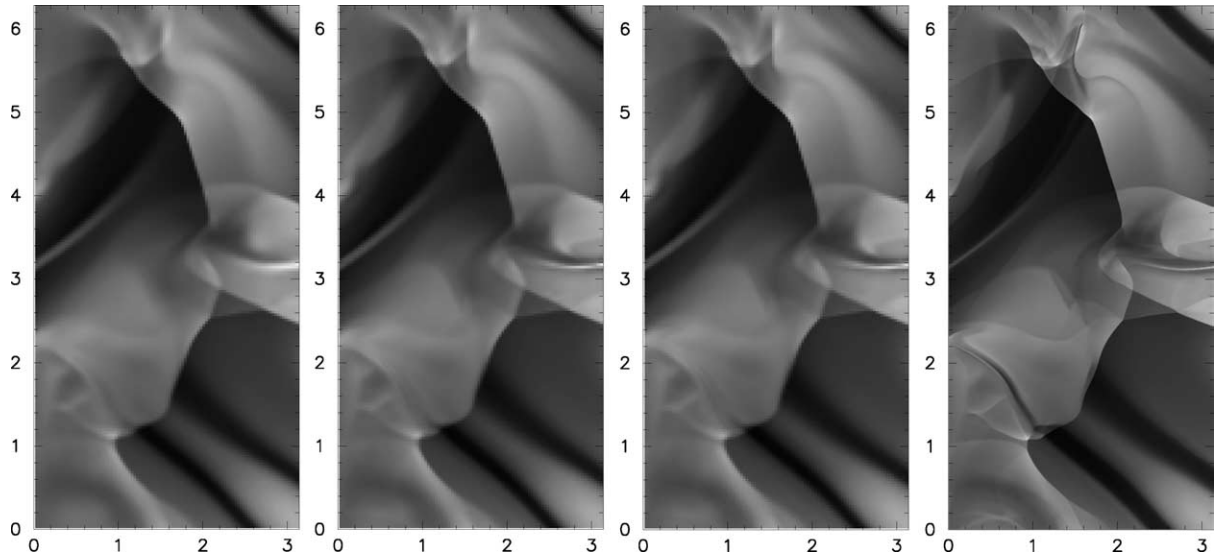

Fig. 12. Gray-scale images of the temperature distribution in the Orszag–Tang vortex problem at $t = \pi$ for (left to right) the HLL solver, the HLLD solver, the Roe scheme at $N = 200$, and the reference solution. The left half of the domain is shown.

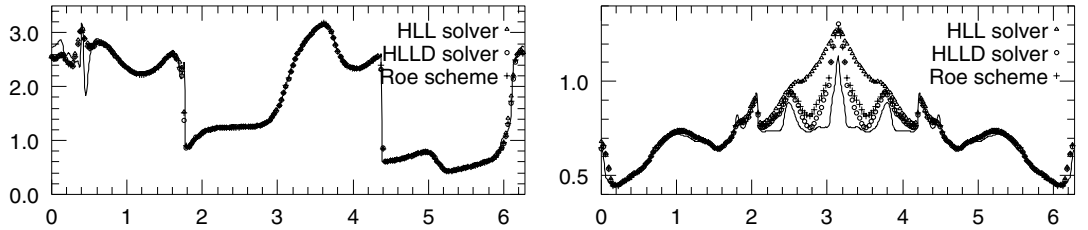

Fig. 13. One-dimensional temperature distribution in the same problem as in Fig. 12 along (left) $y = 0.64\pi$, (right) $y = \pi$. for the HLL solver, the HLLD solver, and the Roe scheme. The solid line shows the reference solution in each panel.

7. Conclusions

We have proposed the multi-state HLL approximate Riemann solver for the ideal MHD equations, named as HLLD approximate Riemann solver. The HLLD Riemann solver was constructed under the assumption that the normal velocity is constant over the Riemann fan. This assumption naturally concluded that the four states approximation in the Riemann fan are appropriate for $B_x \neq 0$, whereas the intermediate states are reduced to the two states when $B_x = 0$. We showed that the HLLD solver can exactly resolve all isolated discontinuities in the MHD system as well as isolated fast shocks. We also proved analytically that the HLLD solver is positively conservative if proper inequalities for the maximum and minimum signal speeds are satisfied. Especially, it was shown that those conditions are quite similar to the conditions for the HLLC solver except for the difference of the expressions for the maximum and minimum eigenvalues. Thus, we considered that the HLLD solver for MHD is a natural extension of the HLLC solver for the Euler equations. Also, several numerical tests demonstrated that the HLLD solver is accurate enough in comparison with the linearized Riemann solver while keeping its robustness. From a typical two-dimensional test, it was considered that the extension to multi-dimensions in the HLLD solver

may be applicable in a similar way as in the linearized Riemann solver. The ratios of CPU time τ for the Orszag–Tang vortex problem at $N = 400$ in our codes are $(\tau^{\mathrm{HLL}}:\tau^{\mathrm{HLLD}}:\tau^{\mathrm{Roe}}) = (1:1.35:2.67)$ in the part of the flux calculation and (1:1.13:1.69) over the whole simulation run, although the actual efficiency for the whole simulation much depends not only on the optimization of the code but also on the algorithm of the divergence cleaning method, the higher-order extension method, the time integration method, and so on. Thus, the HLLD solver seems to be effective particularly in regard to robustness and efficiency rather than the Roe scheme, although exact positivity preserving property in multi-dimensions may not be necessarily assured even in the HLLD solver. Also, the HLLD solver may be applicable to the modified MHD system as subtracting off the background potential field first proposed by Tanaka [28] and applied by many others [18,22,25]. In this modified system, the HLLD solver will be constructed by replacing the total pressure p_{T} with the fluctuating part of the total pressure $\tilde{p}_{\mathrm{T}} = p_{\mathrm{T}} - |\mathbf{B}_0|^2/2$ in (41) for example. A detailed algorithm will be given in the future paper. These all results indicate that the HLLD Riemann solver for the ideal MHD equations can be an alternative to the linearized Riemann solver for MHD.

Acknowledgements

Part of this work was financially supported by the collaboration program of Japan Atomic Energy Research Institute (JAERI), that was arranged by Y. Kishimoto and Y. Ishii of Numerical EXperiment of Tokamak (NEXT) group at Naka Fusion Research Establishment, JAERI. We thank the anonymous reviewers for constructive comments and suggestions improving the readability of the paper.

References

[1] D.S. Balsara, Linearized formulation of the Riemann problem for adiabatic and isothermal magnetohydrodynamics, Astrophys. J. Supp. 116 (1998) 119.
[2] P. Batten, N. Clarke, C. Lambert, D.M. Causon, On the choice of wave speeds for the HLLC Riemann solver, SIAM J. Sci. Statist. Comput. 18 (1997) 1553.
[3] J.U. Brackbill, D.C. Barnes, The effect of nonzero $\nabla \cdot \mathbf{B}$ on the numerical solution of the magnetohydrodynamic equations, J. Comput. Phys. 35 (1980) 426.
[4] M. Brio, C.C. Wu, An upwind differencing scheme for the equations of ideal magnetohydrodynamics, J. Comput. Phys. 75 (1988) 400.
[5] P. Cargo, G. Gallice, Roe matrices for ideal MHD and systematic construction of Roe matrices for systems of conservation laws, J. Comput. Phys. 136 (1997) 446.
[6] W. Dai, P.R. Woodward, An approximate Riemann solver for ideal magnetohydrodynamics, J. Comput. Phys. 111 (1994) 354.
[7] S.F. Davis, Simplified second-order Godunov-type methods, SIAM J. Sci. Statist. Comput. 9 (1988) 445.
[8] A. Dedner, F. Kemm, D. Kröner, C.-D. Munz, T. Schnitzer, M. Wesenberg, Hyperbolic divergence cleaning for the MHD equations, J. Comput. Phys. 175 (2002) 645.
[9] B. Einfeldt, C.D. Munz, P.L. Roe, B. Sjögreen, On Godunov-type methods near low densities, J. Comput. Phys. 92 (1991) 273.
[10] C.R. Evans, J.F. Hawley, Simulation of magnetohydrodynamic flows: a constrained transport method, Astrophys. J. 332 (1988) 659.
[11] S.A.E.G. Falle, S.S. Komissarov, P. Joarder, A multidimensional upwind scheme for magnetohydrodynamics, Mon. Not. R. Astron. Soc. 297 (1998) 265.
[12] J. Gressier, P. Villedieu, J.M. Moschetta, Positivity of flux vector splitting schemes, J. Comput. Phys. 155 (1999) 199.
[13] K.F. Gurski, An HLLC-type approximate Riemann solver for ideal magnetohydrodynamics, SIAM J. Sci. Comput. 25 (2004) 2165.
[14] A. Harten, J.M. Hyman, Self adjusting grid methods for one-dimensional hyperbolic conservation laws, J. Comput. Phys. 50 (1983) 235.
[15] A. Harten, P.D. Lax, B. van Leer, On upstream differencing and Godunov-type schemes for hyperbolic conservation laws, SIAM Rev. 25 (1983) 35.

[16] P. Janhunen, A positive conservative method for magnetohydrodynamics based on HLL and Roe methods, J. Comput. Phys. 160 (2000) 649.
[17] A. Jeffrey, T. Taniuti, Non-linear Wave Propagation, Academic Press, New York, 1964.
[18] A.V. Koldoba, M.M. Romanova, G.V. Ustyugova, R.V.E. Lovelace, Three-dimensional magnetohydrodynamic simulations of accretion to an inclined rotator: the ''cubed sphere'' method, Astrophys. J. Lett. 576 (2002) L53.
[19] S. Li, An HLLC Riemann solver for magneto-hydrodynamics, J. Comput. Phys. 203 (2005) 344.
[20] T.J. Linde, A three-dimensional adaptive multifluid MHD model of the heliosphere, Ph.D. Dissertation, University of Michigan, Ann Arbor, MI, 1998.
[21] T.J. Linde, A practical, general-purpose, two-state HLL Riemann solver for hyperbolic conservation laws, Int. J. Numer. Methods Fluids 40 (2002) 391.
[22] T. Miyoshi, K. Kusano, A global MHD simulation of the Jovian magnetosphere interacting with/without the interplanetary magnetic field, J. Geophys. Res. 106 (2001) 10723.
[23] B. Marder, A method for incorporating Gauss' law into electromagnetic PIC codes, J. Comput. Phys. 68 (1987) 48.
[24] A. Orszag, C.M. Tang, Small-scale structure of two-dimensional magnetohydrodynamic turbulence, J. Fluid. Mech. 90 (1979) 129.
[25] K.G. Powell, P.L. Roe, T.J. Linde, T.I. Gombosi, D.L. De Zeeuw, A solution-adaptive upwind scheme for ideal magnetohydrodynamics, J. Comput. Phys. 154 (1999) 284.
[26] P.L. Roe, Approximate Riemann solvers, parameter vectors, and difference schemes, J. Comput. Phys. 43 (1981) 357.
[27] D. Ryu, T.W. Jones, Numerical magnetohydrodynamics in astrophysics: algorithm and tests for one-dimensional flow, Astrophys. J. 442 (1995) 228.
[28] T. Tanaka, Finite volume TVD scheme on an unstructured grid system for three-dimensional MHD simulation of inhomogeneous systems including strong background potential fields, J. Comput. Phys. 111 (1994) 381.
[29] E.F. Toro, M. Spruce, W. Speares, Restoration of the contact surface in the HLL Riemann solver, Shock Waves 4 (1994) 25.
[30] G. Tóth, The $\nabla \cdot \mathbf{B} = 0$ constraint in shock-capturing magnetohydrodynamics codes, J. Comput. Phys. 161 (2000) 605.